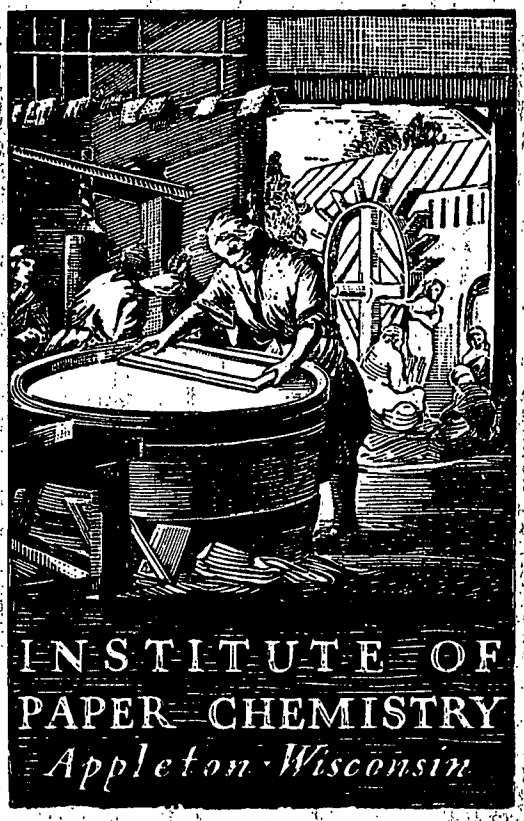

A FUNDAMENTAL RHEOLOGICAL STUDY OF THE BLADE COATING PROCESS

Project 3069

Report Three

A Progress Report

to

MEMBERS OF GROUP PROJECT 3069

May 16, 1975

THE INSTITUTE OF PAPER CHEMISTRY

Appleton, Wisconsin

A FUNDAMENTAL RHEOLOGICAL STUDY OF THE BLADE COATING PROCESS

Project 3069

Report Three

A Progress Report

to

MEMBERS OF GROUP PROJECT 3069

May 16, 1975

MEMBERS OF GROUP PROJECT 3069

Air Products & Chemicals Inc.

Appleton Papers Division

Blandon Paper Company

Champion International

Continental Can Company

Eastex

Great Northern Paper Company

International Paper Company

Mead Corporation

Scott Paper Company

Westvaco Corporation

Weyerhaeuser Company

TABLE OF CONTENTS

THE INSTITUTE OF PAPER CHEMISTRY

Appleton, Wisconsin

A FUNDAMENTAL RHEOLOGICAL STUDY OF THE BLADE COATING PROCESS

SUMMARY

This report contains the results of the initial trials with the IPC Rheometer. The two basic flow geometries investigated were the blade nip (blade angle ten degrees from the tangent) and the "viscometric flow geometry." The latter was considered in several forms, all of which were primarily of the parallel disk or ring geometry. During the trials, consideration was given to the development of experimental techniques, methods of analyzing the data, and the interpretation of results.

Three different types of fluid were used in the testing: Newtonian (glycerin solution), viscous (starch-clay coating), and viscoelastic (polyvinyl alcohol-clay coating).

Generally acceptable results were obtained with the blade geometry. The results were similar to those obtained earlier using 10° blades on the Blade Nip Rheometer. Because of several advantages of the new instrument over the Blade Nip Rheometer, it is probable that it will replace the earlier instrument for all further blade nip measurements.

Two viscometric flow geometries were tested; three ring sections alternating with doctor blades, and three ring sections with angles cut into their leading edges. The data presented in this report were obtained with the latter geometry. Satisfactory viscosity measurements were made on the Newtonian and the viscous fluids. It is presumed that viscosity measurements on the viscoelastic coating would also be satisfactory except at present there is

insufficient information to correct for the torque contributed by the angle part of the geometry. For these viscoelastic fluids it may be necessary to use another geometry, either split ring or ring-blade.

The anticipated use of the viscometric flow geometries to make measurements of viscoelastic normal stresses was unsuccessful. This was apparently due to a tilting of the ring plate relative to the wear plate, which caused pressure and tension forces large enough to mask normal stresses. The tilt, however, apparently did not alter the parallel flow channels sufficiently to distort the torque measurements, thus permitting valid viscosity results to be obtained.

In Progress Report Two a revised theory of nip flow was described. A computer program for applying the theory has been completed. The program has been tested and shown to be operable, but it has not been used extensively to date. The extent of its reliability and usefulness is, therefore, uncertain.

INTRODUCTION

The goals of this research are to develop means for measuring the pertinent rheological properties of coatings, to relate the rheological properties to flow in coating nips, and to investigate the effect of coating formulation on rheological properties.

Work since the last progress report has been mainly concerned with the problem of measuring rheological properties. Prior work with the Blade Nip Rheometer demonstrated that there would probably be difficulties in separating viscous and viscoelastic coating properties using blade nip measurements only. This led to the development of a new test instrument, the IPC Rheometer, in which well-defined viscometric flow could be generated for the separate measurement of viscous shear stress and viscoelastic normal stresses. The new instrument was also designed for blade nip measurements and, since it incorporated several advantages over the Blade Nip Rheometer, it was anticipated that the new machine would completely replace the former device. This report is primarily concerned with the initial evaluation and use of the new rheometer. Extensive consideration is given to the development of experimental techniques, the problems of data analysis, and the interpretation of results. The testing was limited to three fluids of different types: a Newtonian fluid, a viscous coating (starch binder), and a viscoelastic coating (polyvinyl alcohol binder).

In Progress Report Two, the basic principles of a revised theory of flow in nips were described. The theory has since been incorporated into a computer program. The program has been shown to operate successfully, but it has not been sufficiently tested to determine the extent of its usefulness.

THE IPC RHEOMETER

THE NEED FOR A NEW INSTRUMENT

Prior research using the Blade Nip Rheometer demonstrated the advantages of evaluating coating rheology by flow in blade nips (1,2). Unique features not common to other test instruments included shear rates and shearing times comparable to those in coating nips. Also, since the measurements were made in blade nips, a means was provided for investigating the mechanisms of flow in nips under controlled conditions and relating the blade nip flows to coating properties. It became evident in that work that there were advantages that might be gained by continuing research with a new generation of rheometer, the IPC Rheometer. These are, in decreasing order of importance:

1) Contrary to the prevailing theory, there was evidence that viscous and viscoelastic contributions to nip flow behavior might not be separable by nip measurements alone. The IPC Rheometer was designed to permit testing in well-defined viscometric flow as well as in blade nip flow.

2) The volume of test fluid was reduced from about 2.5 liters in the early machine to about 0.9 liter in the new machine.

3) Coating was circulated in the Blade Nip Rheometer by pumping. There was no way to completely flush out the system to avoid contamination of a coating by a prior coating or by cleaning water.

4) The IPC Rheometer is equipped for temperature control while the early instrument was not.

5) There is the potential for more flexibility in the selection of blade geometry with the new instrument.

DESCRIPTION OF THE IPC RHEOMETER

Mechanical Description

A drawing and three photographs of the new instrument are presented in Fig. 1-4. The major parts of the rheometer are described as follows. The part number is followed in parenthesis by those figures in which the part is labeled.

1(1,2,3): Fluid cavity with hollow walls for the circulation of temperature control water. The inside diameter is 20.0 cm. In Fig. 2 the temperature probe can be seen entering through the front of the cavity.

2(1,3,4): Wear plate. The diameter is 14.2 cm.

3(1,3): Shear plate base. The shear plate is screwed to this base within the cavity. Fluid action is generated between the shear plate and the rotating wear plate.

4(1): Roller bearing. This bearing replaced a gimbal bearing called for in the original plans [e.g., see Ref. (2)]. The change was made because a double floating action was observed, caused by the gimbal bearing and the play of the triangular platform on the guide posts.

5(1,2): Air loaded hydraulic ram used to apply normal force to the shear plate.

6(1): Normal force beam. The beam deflection is the measure of normal force.

7(1): Normal force transducer.

8(1,3): Torque beam. The force applied to this beam is a measure of torque applied by fluid forces to the shear plate and fluid cavity.

9(1,3): Torque transducer.

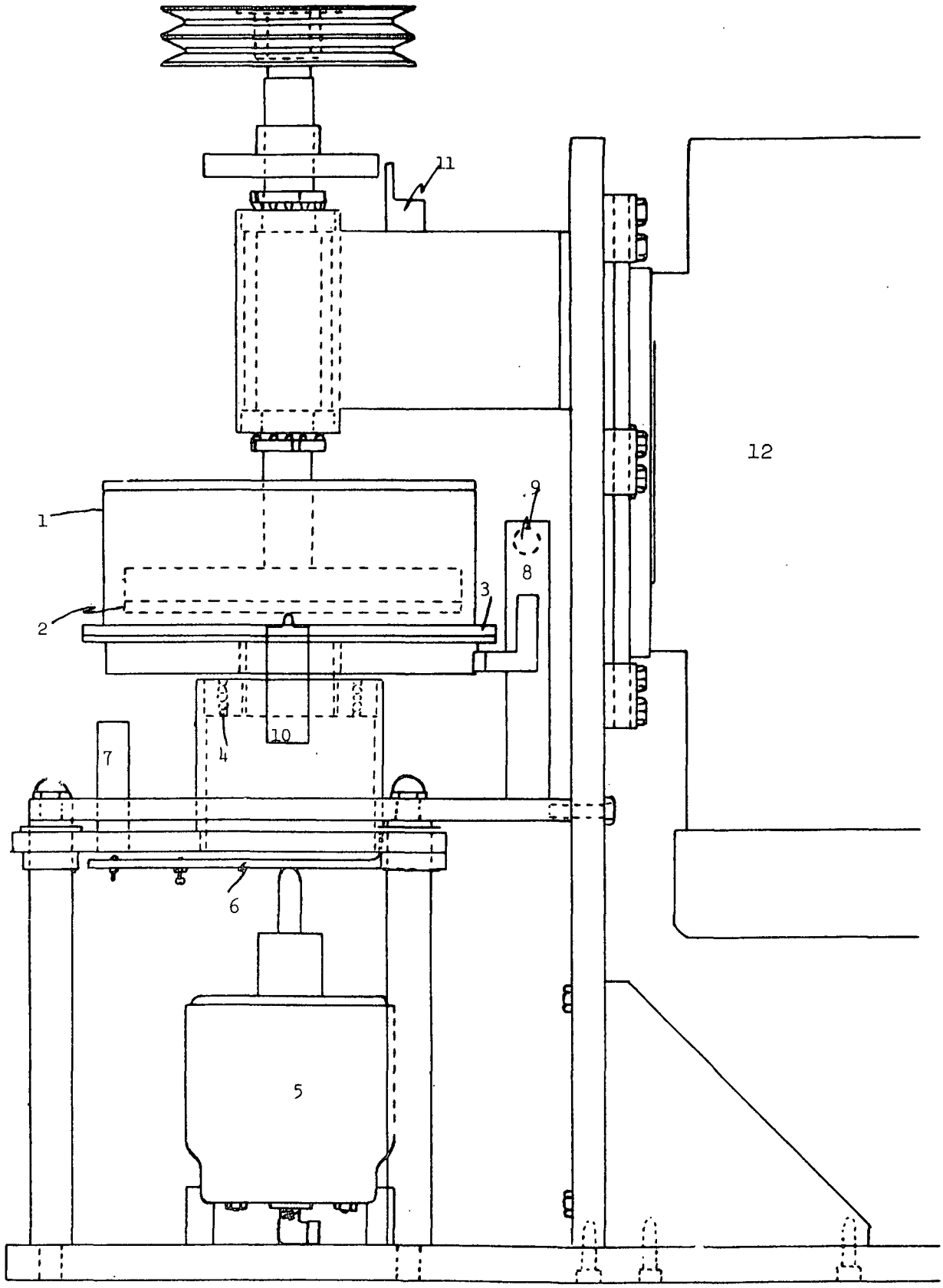

Figure 1. Front View of the IPC Rheometer

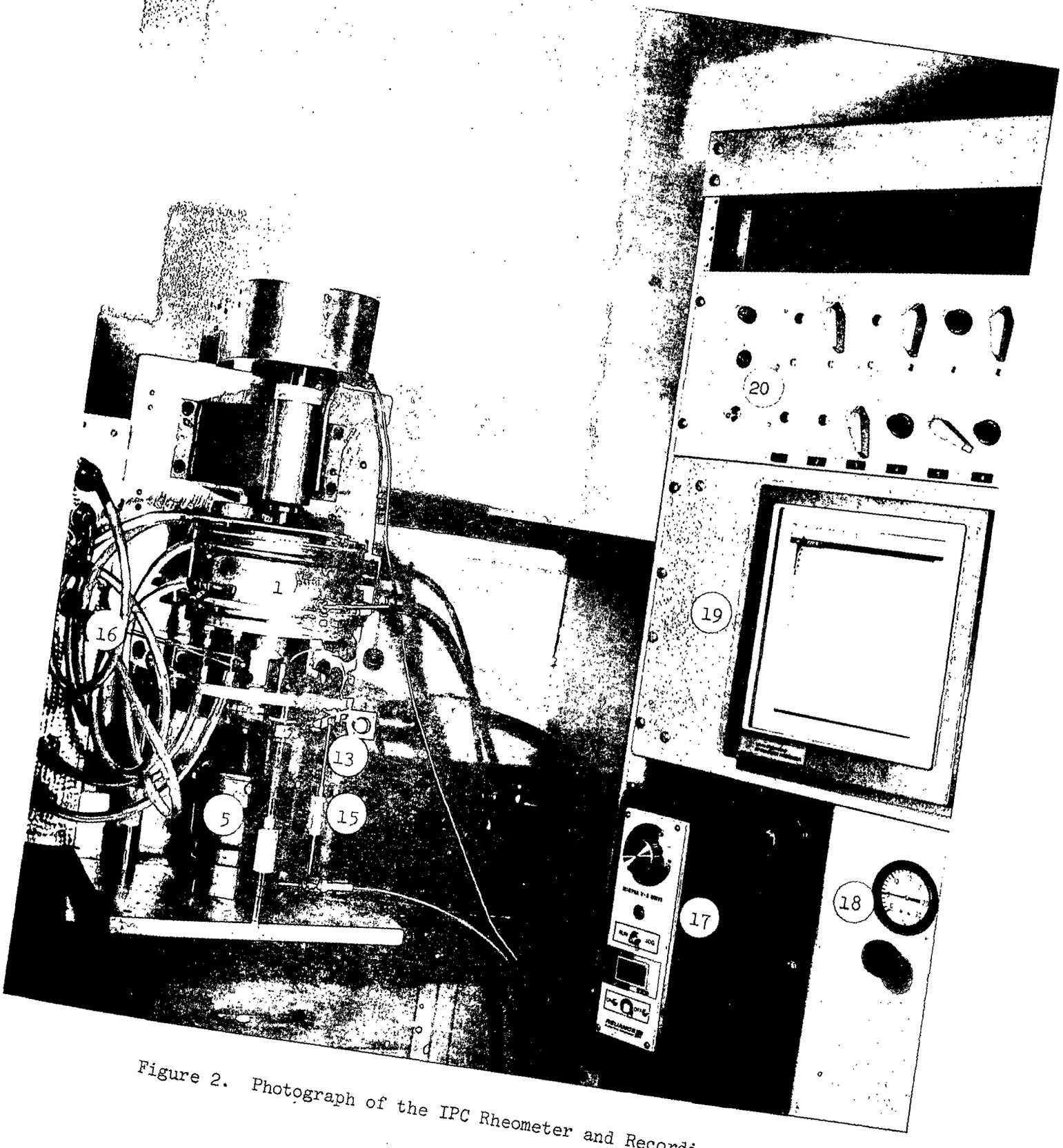

Figure 2. Photograph of the IPC Rheometer and Recording System

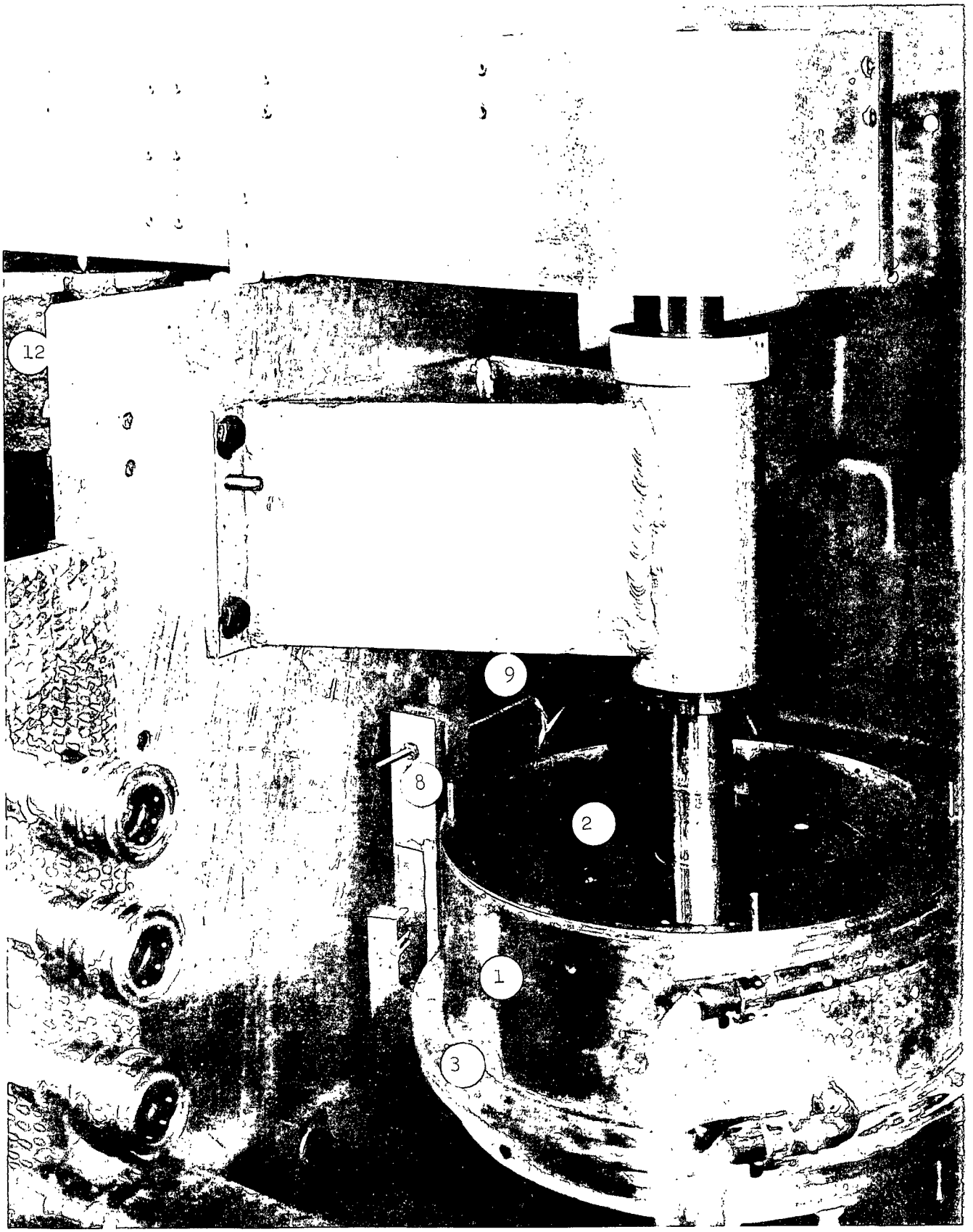

Figure 3. Top View of the Wear Plate in the Fluid Cavity

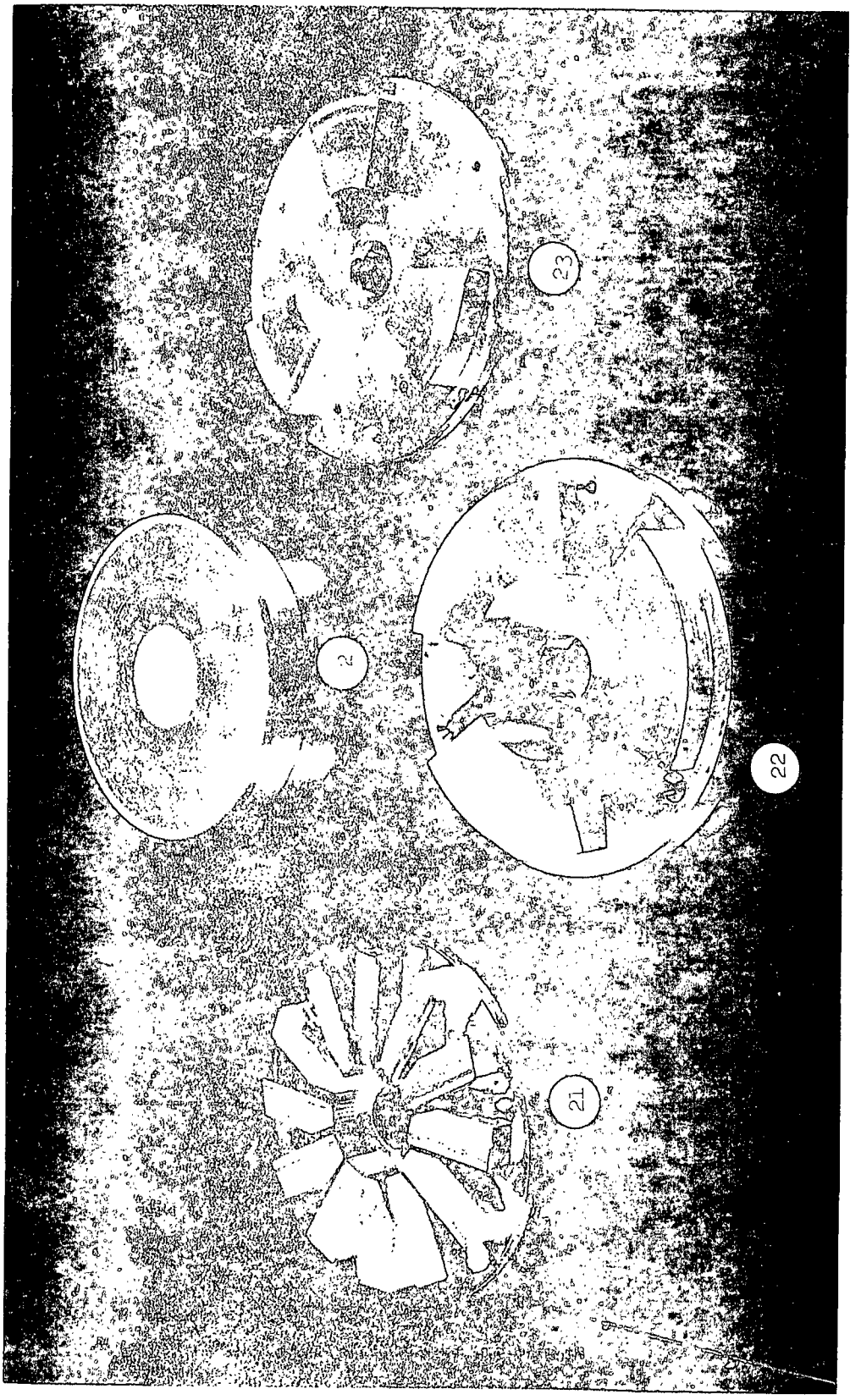

Figure 4. Wear Plate and Three Shear Plates

10(1): Gap transducer. This is a spring loaded transducer permanently attached to the shear plate assembly. The probe must contact the center of the wear plate for best operation.

11(1): Magnetic pick-up. This detects and counts the teeth of the rotating gear, and is calibrated to give rotational speed of the wear plate shaft.

12(1,3): Motor (3 hp.).

13(1,2): Guide post.

14(1): Triangular platform. The platform is free to slide on the three guide posts by means of loosely fitting nylon sleeve bearings.

15(2): One of the collars which can be locked at any position on the guide post. The tape below the collar provides a convenient means of locating the collar position. Each guide post has such a collar.

16(2): Temperature control water circulation lines.

17(2): Motor control unit.

18(2): Pressure valve and gage. The pressure in the hydraulic ram is adjusted here. The gage reading is used for approximate setting of the normal force only.

19(2): Six-point sequential input recorder.

20(2): Controls for setting the appropriate ranges for recorder chart readings.

21(4): Blade geometry shear plate.

22(4): Split ring shear plate.

23(4): Ring-angle shear plate.

Sufficient fluid is enclosed in the fluid cavity to cover the top of the wear plate. This was 900 ml in the work being reported. The fluid is

sheared between the wear plate and the shear plate. The wear plate rotates but has no vertical movement. The shear plate is free to move vertically but is prohibited from rotating. In order to permit close fit between the shear plate and the wear plate, the shear plate assembly is free to "float." During operation the only forces on the shear plate assembly are vertical forces imposed by the hydraulic ram and the fluid being sheared, and torque imposed by the sheared fluid and the contact on the torque beam.

Normal force is applied by the hydraulic ram through the normal force beam. The measurement is made by the normal force transducer. Torque is transmitted through the torque beam and measured by the torque transducer. The gap transducer measures the relative distance between shear plate and wear plate. A zero reading is obtained by contacting the two plates.

Instrumentation

Instead of the 4-channel recorder indicated in the last progress report [Fig. 9, Ref. (2)], a Leeds & Northrup Speedomax multipoint recorder is used. Six sequential points are recorded at a rate of 1.5 sec per point. The chart speed is 60 or 180 inches/hour. There are 100 chart units full scale.

The variable ranges available are as follows:

Point 1: Not currently used.

Point 2: Temperature. Options: 0-100 or 15-65°C full scale.

Point 3: Rotational speed of wear plate. Options: 500 or 2000 rpm full scale.

Point 4: Torque applied to shear plate by fluid. Options 1, 3, 10, 30, 100 in.-lb full scale. Note: As explained in the section on calibrations,

the torque conversion factor is a variable function of the location of the contact on the torque beam.

Point 5: Normal force (lift) applied to the shear plate assembly. Options: 1, 3, 10, 30, 100 lb full scale.

Point 6: Displacement (wear plate-shear plate gap). Options: 0.001, 0.003, 0.01, 0.03, 0.1 cm full scale.

Calibrations

The recorder was calibrated as follows:

Temperature: The cavity temperature probe was factory calibrated.

Wear plate rotational speed: The frequency-voltage converter was set while the speed was indicated with a strobe light.

Normal force: The recorder was set by loading with a dead weight of about 40 lb. Care was required in doing this to avoid friction on the guide posts.

Displacement: The recorder was set by making known displacements on the displacement transducer with a micrometer.

Torque: The relationship between shear plate torque and recorder reading depends on the point of application on the torque beam, as seen in Fig. 3. This will be a function of gap and also depend on the particular shear plate and wear plate used. Thus, there is no one correct recorder calibration, and a calibration was made as a function of position. Torque was applied to the beam by a line passing over a low friction pulley with weights attached. The calibration is given in Table I, with position indicated by the indicator and scale shown in Fig. 3. Note on the figure that the indicator pointer is the center line separating light and dark.

TABLE I

TORQUE CALIBRATION

Scale Reading, cm	Torque/($\underline{T}$ $T_{\underline{c}}$)[a], in.-lb.	Torque/($\underline{T}$ $T_{\underline{c}}$), erg
0.55	0.500	0.565×10^{6}
1.41	0.579	0.655
2.30	0.670	0.757
3.23	0.800	0.904
4.10	0.968	1.093
4.97	1.240	1.402

[a] $\underline{T}$ is the chart reading (full scale = 100) and $T_{\underline{c}}$ is the range setting, labeled in in.-lb.

DESIGN OF VISCOMETRIC FLOW SHEARING PLATES

Basic Disk and Ring Geometries

It is required that a flow field be set up which is known to be viscometric and which permits the measurement and interpretation of forces resulting from the flow. Forces resulting from secondary flows in the system, even if partially viscometric, must be measurable so that appropriate corrections can be made to the total measured forces.

As a starting point, the disk and ring geometries illustrated in Fig. 5 were considered. The desired viscometric flow is generated in the primary film of each geometry. The primary film is that fluid which is enclosed by the primary surface of the shear plate and the wear plate. Initial estimates of the variable ranges possible with these geometries indicated no strong preference of one over the other.

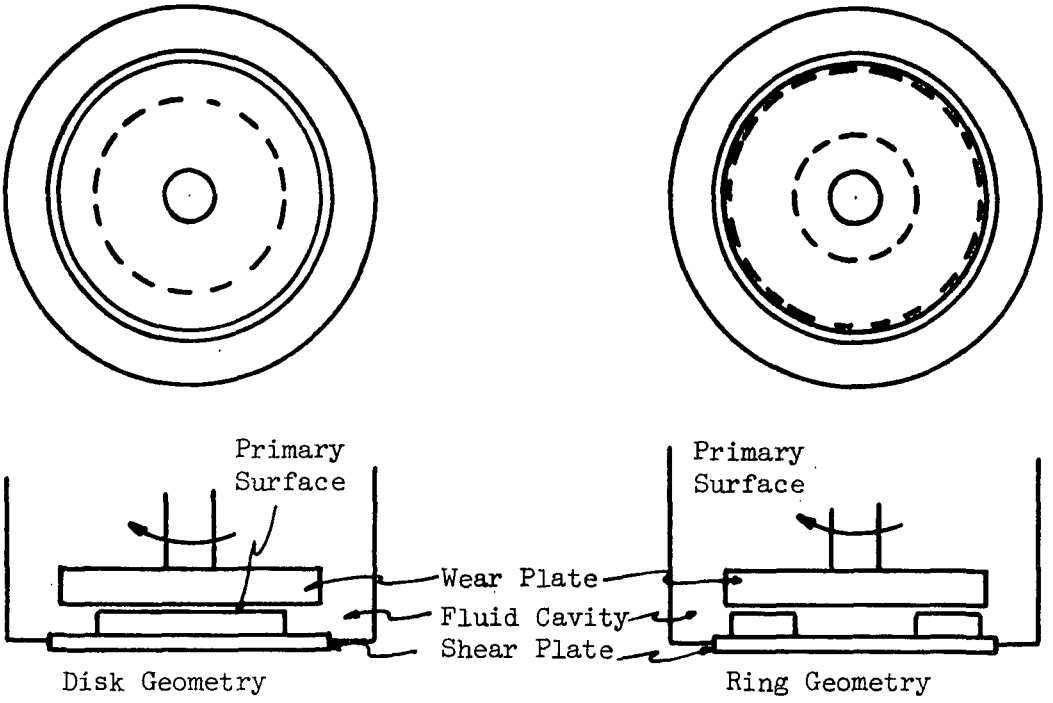

Figure 5. Basic Shear Plate Designs

Angular momentum effects may be used to set a practical upper limit to the ring or disk outside radius. In theory, the fluid enclosed between a stationary and a rotating disk causes a normal force between them. Averaging the fluid velocity across the fluid film (3,4), this force would be:

$$\text{Force} = \pm \frac{\pi \rho \omega^2 R_o^4}{12} \qquad (1)$$

in which ρ is the fluid density, ω is the rotational speed of the rotating disk, and R_o is the radius of the disks. The force is positive or negative depending on whether ambient pressure is at the edges or the center of the fluid. Since normal force measurements would be used in determining viscoelastic normal stresses the corrective force of Equation (1) should have a reasonable upper limit. An analysis of several factors, including maximum shear rate attainable, viscous heat problem, and the angular momentum effect, led to estimates of maximum rotational speed of about 80 rad./sec (765 rpm)

and an optimum radius of the disk or ring of about 7 cm. These values would give rise to a maximum corrective force of about 13 lb. The presumed drastic increase in corrective force with increased ω or R_o is evident from Equation (1). Subsequent experiments have shown that the corrective force is much smaller than predicted. This means that the angular speed may be increased to the machine limits. The radius limit of 7 cm is still considered optimum.

Split Ring Geometry

The fluid cavity walls and cover, and the shear plate support, are temperature controlled by water circulation. To minimize temperature increases due to viscous heating, it was considered desirable to use all of the fluid in the cavity for testing, not just a thin film. This would greatly increase the heat transfer surface area and result in a test volume of large heat content.

The requirement of continual renewal of the fluid test film by the bulk fluid in the cavity led to the concept of a split ring geometry, illustrated in Fig. 6. This geometry, instead of a disk or continuous ring, also has other potential advantages. In conventional viscometers the shearing energy is put into extremely small fluid volumes over long time periods, resulting in thixotropic breakdown. This is completely unrealistic in comparison to the short duration of fluid deformation prevalent in coating nips. The effect of a split ring geometry should be to spread out the energy input over a large fluid volume and thus better approximate coater operation. The split ring geometry also affects the response time of the equipment. In the course of an experiment the film thickness is frequently changed. This needs to be done in a reasonable time to facilitate the taking of data and to reduce the overall effect of viscous heating. The use of three ring sections accomplishes this, since there is continuous fluid flow into the sheared films. Thus, a

change in film thickness does not depend on slow flow out the edges of a continuous ring or disk.

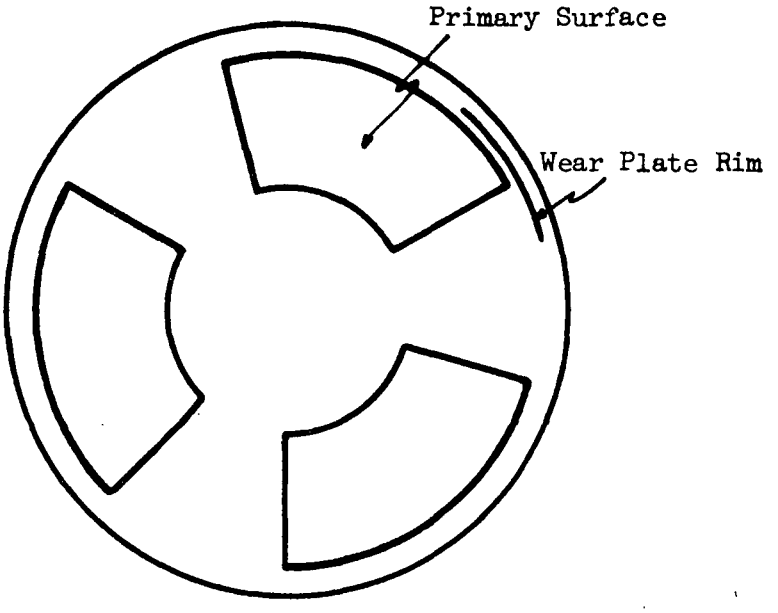

Figure 6. Split Ring Shear Plate Geometry

Ring-Blade Geometry

Successful operation of the rheometer requires that the shear plate and the wear plate remain parallel during operation, and that there be some way to fix and hold constant the film thickness. In the conventional viscometer these requirements are met by rigidly fixing the position of both shearing surfaces. Operating the rheometer with blades on the shear plate, the required stability and control is provided by the lubricating action of the blade doctoring. Operating with a viscoelastic fluid in the ring geometry in Fig. 6, comparable stability would result from viscoelastic normal stresses. For viscous fluids, however, there is no apparent reason for the ring geometry to operate satisfactorily. To provide the required effect, low angle blades were placed between ring sections as shown in Fig. 7. This latter geometry was the first to be constructed and tested experimentally.

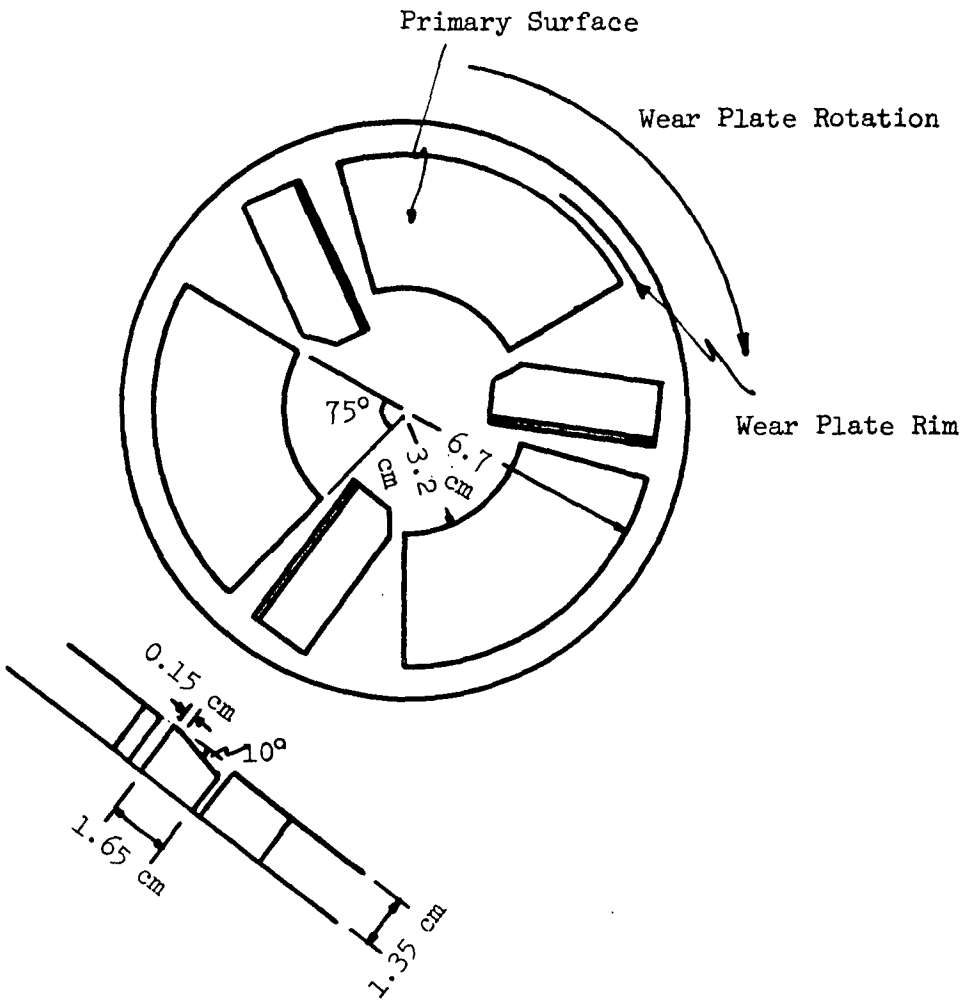

Figure 7. Ring-Blade Shear Plate Design

The Tilt Phenomenon with the Ring-Blade Geometry

During the initial experimental tests of glycerin solutions with the ring-blade geometry of Fig. 7, it was found that the film thickness was generally much greater than predicted based on prior experiments with the blade geometry. On analyzing the results it was concluded that normal forces generated by the three blades alone could not be sufficient to account for the large gap values, and that some other agent must be responsible. Further consideration led to the conclusion that such forces could only be generated by a tilt in the shear plate relative to the wear plate.

Consider Fig. 8 to see how such a tilt might arise. Assume that a small perturbation of the shear plate results in a reduction in film thickness at a and an increase at d. The stabilizing effect of the blades would result in an increase in normal force at blades b and f and a decrease at blade d, tending to cause a compensating tilt of the shear plate back to parallel. The effect on the ring sections would be different, however. The presumed perturbation would result in diverging flow at section c and converging flow at section e. The resulting tension at c and pressure force at e would not tend to restore the shear plate to parallel but would cause the tilt to shift clockwise around the shear plate. Obviously this would be a very complex system to describe in detail. It would depend on the mass distribution of the shear plate assembly, the fluid forces involved, the speed of rotation, and other factors. It is also conceivable that under some conditions the net effect would be to cause a lower than expected film thickness, rather than greater, since there are forces of tension as well as pressure involved. The experience to date suggests that the net effect is to increase the force and, thus, the film thickness.

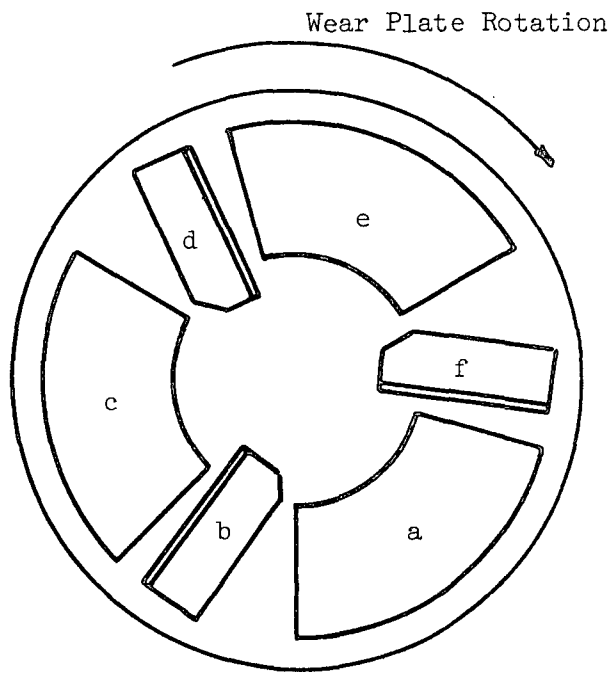

Figure 8. Figure Used to Illustrate Shear Plate Tilt

Ring-Angle Geometries: Implications of the Tilt Phenomenon

It was thought possible that the tilt effect could be reduced or eliminated by locating the stabilizing points at the ring sections instead of the blades, since the unstabilizing effect is located at the ring sections. This was done by removing the blades and cutting angles in the leading edges of the ring sections as shown in Fig. 9. The experimental behavior was not appreciably changed. Another attempt to reduce the tilt effect was made by shortening the ring sections as shown in Fig. 10, again without apparent success.

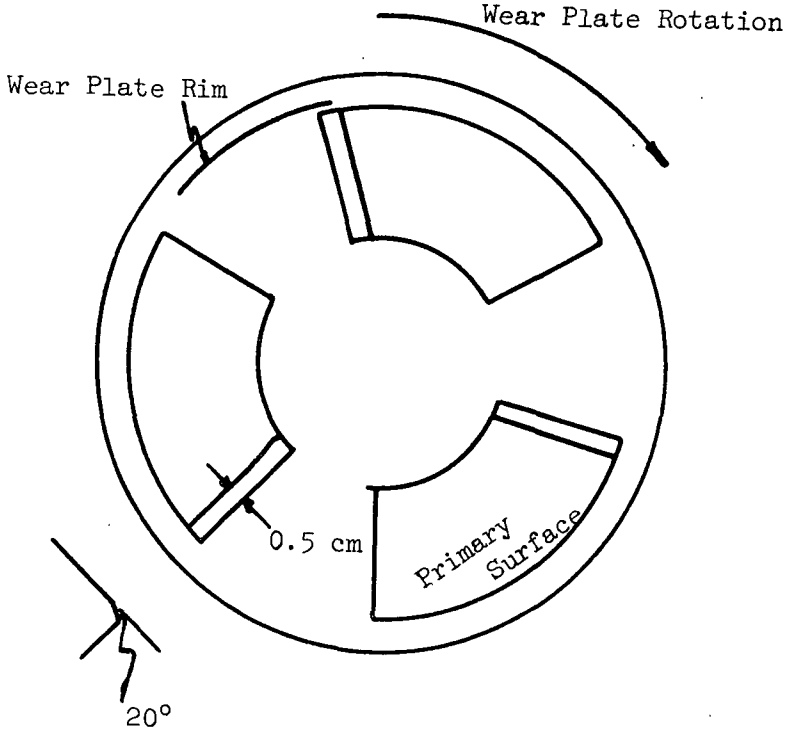

Figure 9. Ring-Angle Shear Plate Geometry

Because of this unanticipated effect, it appears doubtful at the present time that any of the shear plate geometries considered can be used to determine viscoelastic normal stresses. Further work may clarify this point and hopefully produce a more optimistic outlook. The effect has also resulted in a reduction of maximum shear rate by a factor of about three, from the anticipated value of about 10^6 sec^{-1}.

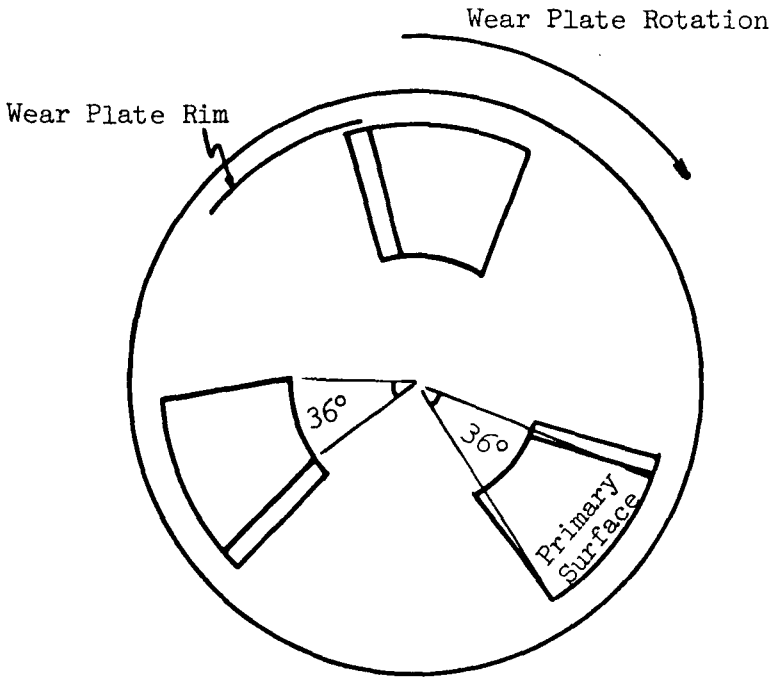

Figure 10. Shortened Ring Sections

On the other hand, viscosity results have not been significantly affected by the tilt phenomenon, for two apparent reasons:

1) It can be shown that the normal force resulting from slight convergence or divergence in flow channels of large length thickness ratios is very large compared to the effect on drag forces. The viscosity function is determined by the drag forces.

2) Apparently the fluid tension created by diverging flow is insufficient to cause film split of sheared films with consequent erroneous torque measurements.

DESIGN OF BLADE GEOMETRY SHEARING PLATE

Factors that went into the design of the first blade shearing plate were:

1) As shown in the discussion of the effect of angular momentum for the viscometric flow shearing plates, a practical limit of about 7 cm was fixed for the shear plate geometry. The effect of angular momentum was expected to be, as an estimate, about the same for all plate geometries and this fixes the same diameter for the blade plate.

2) Extensive work was done on the Blade Nip Rheometer using 10° blades (1). The first blade shearing plate for the IPC Rheometer was made with the same angle blades so that there would be a useful basis for comparing results.

3) Analysis of the variable ranges expected favored a large number of blades on the shearing plate. A large number was also desired in order to reduce the importance of corrective forces resulting from secondary flows. The practical limit on the number of blades is 12, for geometric reasons.

These factors led to the design and construction of the blade shearing plate shown in Fig. 11.

OPERATING PROCEDURES

Initial Comments

At this stage of the research, experimental techniques are continually evolving toward an acceptable optimum. The procedures described here are those which are considered best at this time. Some of the experimental results were obtained using earlier techniques and, where it is considered likely that a change in technique would cause a change in results, this will be noted in the later discussion of results.

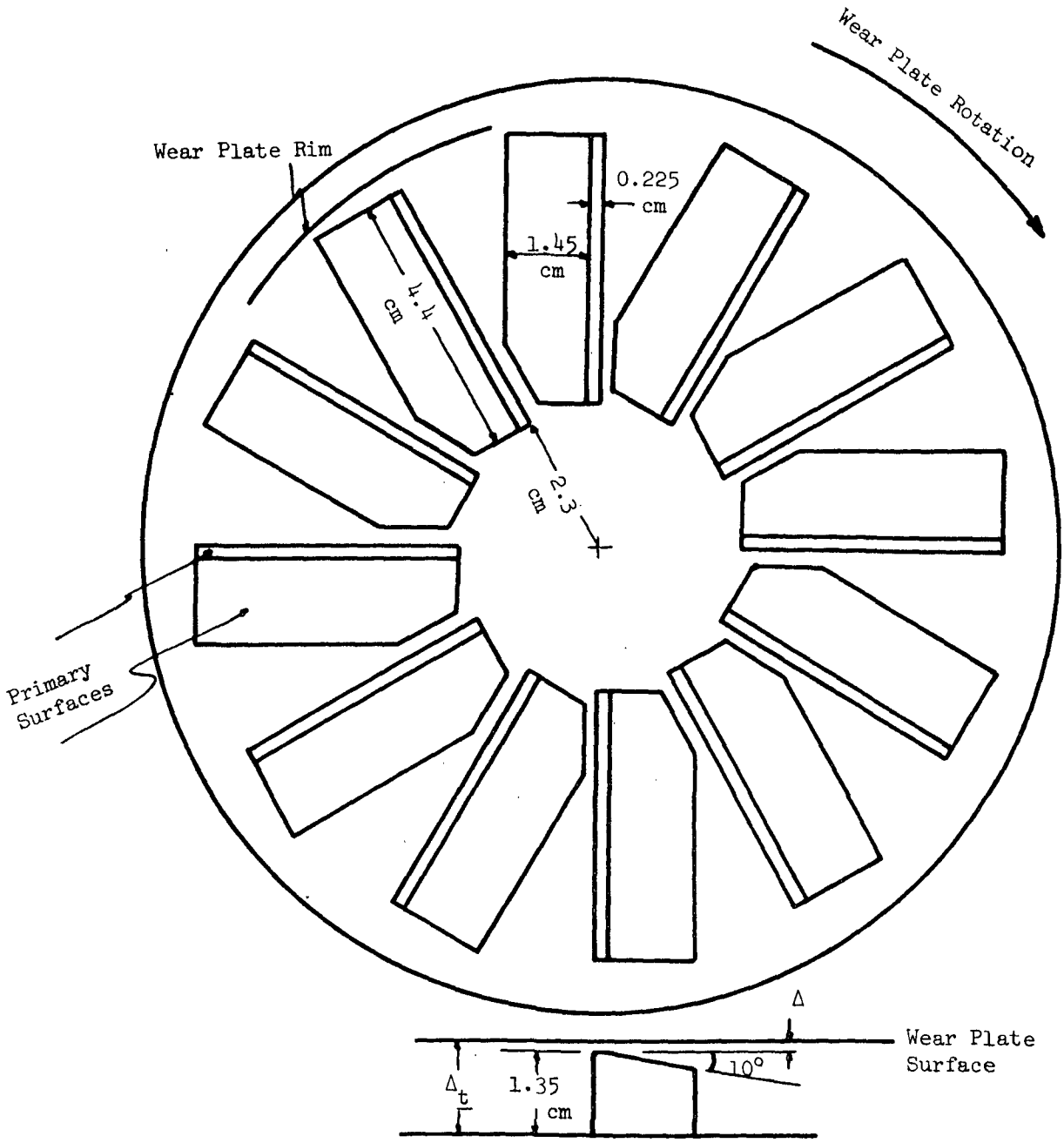

Figure 11. Shear Plate with Twelve 10° Blades

Grinding in Shearing Plates

Both blade and ring-type shearing plates were ground in with the wear plate. Water slurries of 400 grit Carborundum were used. Approximate conditions used were 25 lb normal force and 150 rpm rotational speed. Grinding in blades was fairly quick and easy, with total grinding time of the order of 15-30 min. Grinding rings required several hours due to the large surface areas. In all cases the grinding was limited to no more than one minute before replenishing the Carborundum.

Procedures Required at the Start of an Experiment

1) Start the temperature control water circulating. A sink is being used as a water bath, with tap water run in to adjust to the desired temperature. It may be desirable later to use heaters and a temperature regulator. Water is circulated by a submersible Teel pump at a rate of about one gal/min.

2) Add 900 ml of test fluid to the fluid cavity.

3) Adjust the zero normal force reading. This is done with the shear plate assembly completely supported by the hydraulic ram and negligible friction on the guide posts. This position is reached by careful manual manipulation of the pan. The zero load reading is set at 10 on the chart (full scale 100) to assure measurement of negative values.

4) Adjust the rotation of the pan so that contact is just made with the torque beam. This is done by applying a torque to the shear plate assembly with a rubber band.

5) For each shearing plate a static calibration of normal force *vs.* displacement should be available. This may be done at the start of an experiment but is not necessary every experiment.

6) Assure that the system is at the desired temperature throughout. A good check of this is to rotate the wear plate to mix the fluid in the cavity and compare the recorded (fluid cavity) temperature with that of the circulating water.

The Large Gap Test

It is necessary to correct experimental data for secondary flow effects. This is done by using results obtained with very large primary film thicknesses, of the order 0.15 to 0.6 cm.

There are two options for the large gap test which is run at the start of the experiment:

1) If normal force data are to be used, the gap values (Δ) are set by lines scribed on the hydraulic ram. Gaps of 0.2, 0.4, and 0.6 cm are sufficient. Normal force ($\underline{F}$) and torque ($\underline{T}$) are measured as functions of speed (ω). This is the "floating" technique.

2) If normal force data are not to be used, the gaps are set by raising the shear plate to the wear plate, raising the collars on the guide posts up known distances from the shear plate assembly by inserting shims, and locking the collars. The shear plate assembly is then lowered to leave the desired gap. This approach gives more stable operation than the first and is preferred. If normal force data are used it may be desirable to use both techniques to assure the best possible torque values. Torque is measured as a function of speed. Shims are available to set gaps of 0.159, 0.218, and 0.477 cm. This is the "nonfloating" technique.

Testing Procedure

The coating evaluation is done in several runs; with normal force ($\underline{F}$) as a parameter, speed (ω) as the independent variable, and torque ($\underline{T}$) and gap (Δ) as dependent variables. The zero gap reading ($\underline{\Delta_o}$) is set at the start of a run and also checked at the end. Care must be taken to assure that sufficient time is allowed in order to squeeze essentially all fluid from the shear plate-wear plate channels and surface contact is made. For runs made at normal force values less than 20 lb, $\underline{\Delta_o}$ is determined at 20 lb to assure good fit of the two plates. The zero torque value ($\underline{T_o}$) is set at the start of a run and can be checked during the run by backing off of the torque beam. The torque sensitivity range can be changed during a run but the displacement range remains constant during a run.

Data are recorded by continuous cycling in the following order:

Point 1: Currently not used.

Point 2: Temperature (θ).

Point 3: Rotational speed (ω).

Point 4: Torque ($\underline{T}$).

Point 5: Normal force ($\underline{F}$).

Point 6: Displacement (Δ).

The following procedure is used to obtain a data set within a run:

1) Set the recorder at ω.

2) Set the speed dial at the desired level.

3) Start the motor using the fast start jog switch.

4) When ω is seen to be stable (1-2 sec), record ω, $\underline{T}$, $\underline{F}$, and Δ and stop the motor. The recorder is left on to record θ and is then stopped

at ω for the next data set. To check the zero torque or change the torque sensitivity range, run the recorder to $\underline{T}$ and then back to ω, with the motor not running.

For particular values of ω and $\underline{F}$ there will be an equilibrium value of Δ. When the motor is started this value of gap will be reached quickly, but not instantaneously, and care must be taken that data are not recorded before it is reached. The best monitor for this is to observe the behavior of the torque reading on the recorder. If it is changing rapidly, then equilibrium has apparently not yet been reached, and the recorder can be stopped for a moment until it is. Such a change in torque must not be confused with a slow change due to viscous heating or other spurious effect. Experience to date indicates that the time to reach and record a stable ω is sufficient to reach the equilibrium value for $\underline{T}$ and, thus, Δ.

ANALYSIS OF DATA

INTRODUCTION

There are two parts to the analysis of data: the separation of "primary" fluid forces from the total measured forces, and the analysis of the primary forces to yield fluid properties or establish basic principles of flow. Primary forces are defined as torques and normal forces resulting from flow between the wear plate and the "primary" surfaces of the shear plates. The latter are illustrated in Fig. 11 for the blade geometry and in Fig. 5, 6, 7, 9, and 10 for the viscometric flow geometries. The remaining forces are "secondary" and are of two types. The first type are those forces which are presumed to be relatively insensitive to changes in gap. These include forces resulting from flows inside, outside, and between rings and blades, flows between the wear plate and the fluid cavity, and various edge effects. These secondary forces are determined from large gap experiments, in which the primary forces become relatively small. The second type of secondary forces are those resulting from blade flow in the ring-blade geometry of Fig. 7 and those resulting from converging flow in the angles of the ring-angle geometries of Fig. 9 and 10. These forces are determined by independent blade geometry experiments (ring-blade geometry) or by theoretical descriptions of converging flow (both geometries).

There are two presumptions implied in the preceding discussion: first that one can determine well-defined secondary forces with reasonable accuracy, and, second, that there are no interactions between primary and secondary forces. The validity of these presumptions must be evaluated continually as data are analyzed.

ANALYSIS OF PRIMARY RESULTS

Viscometric Flow Geometries

Because of the previously discussed tilt effect, the normal force data for these geometries are not considered useful and, for the present, torque data only are considered.

The object of the analysis is to determine fluid viscosity as a function of shear rate. The major problem is that for any particular set of experimental variables the shear rate is not constant throughout the primary film but varies from the minimum at the inside radius to the maximum at the rim Two methods of determining viscosity as a function of the maximum shear rate will be described. For the first method it is necessary to assume both the flow behavior in the film and the form of the viscosity-shear rate dependence. The first method is a one step analysis. The second method is a two step analysis. In the first step one determines shear stress as a function of maximum shear rate, without assuming any viscosity-shear rate functionality. It is not necessary to assume the type of flow in the film but a restricting assumption is made which will be described later. In the second step, one assumes a velocity profile across the film to determine viscosity as a functior of maximum shear rate.

It is anticipated that comparable viscosity results will be obtained with the two methods of analysis for most coatings. The question of which to use may depend on the convenience of making the calculations.

The First Method of Analysis

It is assumed that flow in the primary films is viscometric and that the velocity profiles are linear. Converging flow prior to the primary

surfaces of the ring-angle geometry will cause deviation from the linearity of the profile but this will be negligible for film thicknesses as small as those being considered. Deviations from the presumed parallel flow channels and linear velocity profiles, due to the tilt effect, can only be checked by considering final results, and it will be seen that the assumptions appear to be reasonable for small gap values.

The geometry of any of the disk or ring devices can be described by the following terms. The numerical values in parenthesis are for the ring-angle geometry of Fig. 10.

Φ = total ring angle ($3 \times 36^\circ = 1.887$ radians),

$\underline{R_i}$ = inside radius of the ring sections (3.2 cm),

$\underline{R_o}$ = outside radius of the ring sections (6.7 cm),

$\underline{H}$ = height of the ring sections (1.35 cm),

Δ = film thickness (gap), experimental variable,

$\Delta_t = \Delta + \underline{H}$ = estimate of the "secondary flow" gap,

$\underline{r}$ = variable radius, and

ω = rotational speed of the wear plate, experimental variable.

It is convenient to assume a power law fluid:

$$\tau = \eta_o \Gamma^n = \eta\Gamma \qquad (2)$$

in which η_o and $\underline{n}$ are fluid parameters, τ is shear stress, η is the variable viscosity, and Γ is the shear rate defined by:

$$\Gamma = \omega\, r/\Delta \qquad (3)$$

The maximum shear rate occurs at the outer rim of the rings and is:

$$\Gamma_m = \omega R_o/\Delta \qquad (4)$$

For particular values of ω and Δ, the shear rate, Γ, varies from $\omega R_i/\Delta$ to Γ_m. For a given fluid, the parameters n and η_o may also be functions of shear rate. In using the power law expression, however, it is only required that n and η_o be approximated by constants over the limited shear rate range under examination. Such an approximation is almost always valid over shear rate ranges as limited as those encountered in this work [Γ (maximum)/Γ (minimum) = 6.7/3.2 $\approx$ 2].

A differential torque balance is set up:

$$d T_p = \Phi \tau r^2 dr \qquad (5)$$

in which T_p is the torque due to flow in the primary film. Substituting Equation (2) and (3) into (5) and integrating:

$$T_p = \Phi \eta_o (\omega/\Delta)^n \int_{R_i}^{R_o} r^{2+n} dr$$

$$= [(\Phi \eta_o)/(3+n)](\omega/\Delta)^n (R_o^{3+n} - R_i^{3+n}) \qquad (6)$$

Or, in terms of the variable and maximum shear rate:

$$T_p = [\Phi/(3+n)][(R_o^{3+n} - R_i^{3+n})/r^n] \eta \Gamma$$

$$= [\Phi/(3+n)][(R_o^{3+n} - R_i^{3+n})/R_o^n] \eta_m \Gamma_m \qquad (7)$$

in which η_m is the viscosity at the maximum shear rate, Γ_m.

For a given fluid the parameter n can be determined from the slope of a log-log plot of T_p vs. ω/Δ. For the coatings considered in this report, n was constant over the entire range of variables. For a Newtonian fluid n is equal to 1. Equations (4) and (7) are then used to calculate the viscosity as a function of the maximum shear rate.

The Second Method of Analysis

In the first step of the analysis, the shear stress is determined as a function of the maximum shear rate. In doing this it is assumed that, for a given film thickness, the shear stress is a unique function of the point velocity of the rotating wear plate, independent of the rate of rotation and the radius considered.

Integration of the torque balance of Equation (5) is carried out:

$$T_p = \Phi \int_{R_i}^{R_o} \tau\, r^2\, dr \qquad (8)$$

A change of variable is made from r to v, the velocity at the wear plate surface. The variable change is made as follows:

$$\left.\begin{aligned} v &= \omega\, r \\ dv &= \omega\, dr \\ \omega &= V_o/R_o \\ r^2\, dr &= (v^2/\omega^3)dv = (R_o{}^3/V_o{}^3)v^2\, dv \end{aligned}\right\} \qquad (9)$$

in which V_o is the velocity at R_o. The last Equation (9) is substituted into Equation (8):

$$T_p = (R_o/V_o)^3\, \Phi \int_{V_i}^{V_o} \tau\, v^2\, dv \qquad (10)$$

in which V_i is the velocity at R_i.

The differentiation of Equation (10) with respect to V_o serves to remove the shear stress from the integral. The film thickness, Δ, is held constant while V_o, and thus ω, is varied. The differentiation gives the following results:

$$dT_p/dV_o = \Phi(R_o/V_o)^3 \frac{d}{dV_o} \int_{V_i}^{V_o} \tau\, v^2\, dv + R_o^3\, \Phi \left[\int_{V_i}^{V_o} \tau\, v^2\, dv\right] \frac{d}{dV_o}\left[\frac{1}{V_o^3}\right]$$

$$= \Phi(R_o/V_o)^3 \left[\tau(V_o)V_o^2 - \tau(V_i)V_i^2 \frac{dV_i}{dV_o}\right] - 3\Phi \frac{R_o^3}{V_o^4} \int_{V_i}^{V_o} \tau\, v^2\, dv$$

$$= \Phi \frac{R_o^3}{V_o}\left[\tau(V_o) - \tau(V_i)\left(\frac{V_i}{V_o}\right)^2 \frac{dV_i}{dV_o}\right] - 3\Phi\left[\frac{R_o^3}{V_o^4}\right]\left[\frac{V_o^3}{\Phi R_o^3}\right] T_p \qquad (11)$$

Since

$$dV_i/dV_o = V_i/V_o = R_i/R_o,$$
$$d\log(V_o) = d\log(\omega),$$
$$\tau(V_o) = \tau(R_o) = \tau_o,$$
$$\tau(V_i) = \tau(R_i) = \tau_i;$$

Equation (10) can be rearranged to give:

$$\tau_o - (R_i/R_o)^3\, \tau_i = [3\, T_p/(R_o^3\, \Phi)]\, [1 + (\tfrac{1}{3})d\log(T_p)/d\log(\omega)] \qquad (12$$

All quantities in Equation (12) except τ_o and τ_i are experimentally determined. A trial and error solution is required to determine τ_o. This would converge in one or two trials since $\tau_i/\tau_o < 1$ and $(R_i/R_o)^3 \ll 1$. The shear rate is then determined from Equation (4) and the desired viscosity is given by:

$$\eta_m = \tau_o/\Gamma_m \qquad (13$$

Blade Geometry

With the blade geometry, both torque and normal force data are believed to be valid. As with the viscometric flow geometries, there are two methods of analyzing blade nip data. The first method is a one-step process in which a type of fluid behavior and a theory of nip flow are assumed. The type of results obtained from the analysis can vary. In the present case, two possibilities will be described; the calculation of torque and normal force values which can be compared with experimental values to test the theory of nip flow, and the calculation of fluid viscosity as determined separately by torque and normal force data. The second method of analysis is a two-step process. In the first step the data are transformed from torque and normal force as functions of rotational speed to tangential and normal force, per blade width, as functions of the maximum (rim) velocity of the wear plate. The derived forces can be used in the second step to test theories or to determine apparent viscosity values. Since the derived forces per blade width are comparable to results obtained with the Blade Nip Rheometer (1), they can be used for comparison without recourse to a second step in the analysis. Because of the utility of the intermediate results of the analysis, it is probable that the second method of analysis will be followed in treating future blade nip data.

The First Method of Analysis

The fluid is assumed to be described by a power law, as described in Equation (2). Flow is assumed to be viscometric. These assumptions permit the calculation of drag and normal force functions, $\underline{D}(\underline{n},\Delta)$ and $\underline{F}(\underline{n},\Delta)$, respectively. Δ is defined as the film thickness under the blade tip. These functions are independent of velocity and the power law coefficient, $\eta_{\underline{o}}$. If the exponent $\underline{n}$ is to be determined by the data being analyzed, the calculations are of a

trial and error nature. If n is known from some other source, then the calculations are not trial and error. The functions mentioned above are defined by fluid forces exerted on the blade nip, as follows:

$$\text{drag force/blade width} = \eta_o \, v^n \, D(n,\Delta) \tag{14}$$

$$\text{normal force/blade width} = \eta_o \, v^n \, F(n,\Delta) \tag{15}$$

in which v is the linear speed of the moving surface of the nip. Since Δ is constant for a particular set of data, $D(n,\Delta)$ and $F(n,\Delta)$ are also constant and torque and normal force balances are derived from Equations (14) and (15):

$$d\,T_p = \eta_o \, v^n \, r \, D(n,\Delta) \, dr \tag{16}$$

$$d\,F_p = \eta_o \, v^n \, F(n,\Delta) \, dr \tag{17}$$

in which T_p and F_p are torque and normal force resulting from the blade doctoring action. Velocity is a function of radius:

$$v = \omega \, r \tag{18}$$

Thus:

$$d\,T_p = \eta_o \, \omega^n \, r^{n+1} \, D(n,\Delta) \, dr \tag{19}$$

$$d\,F_p = \eta_o \, \omega^n \, r^n \, F(n,\Delta) \, dr \tag{20}$$

Integrating and adding the results for all blades:

$$T_p = N \, \eta_o \, \omega^n \, D(n,\Delta) \int_{R_i}^{R_o} r^{n+1} \, dr$$

$$= \frac{N \, \eta_o \, \omega^n \, D(n,\Delta)}{n+2} \left(R_o^{\,n+2} - R_i^{\,n+2}\right) \tag{21}$$

$$F_p = N \eta_o \omega^n F(n,\Delta) \int_{R_i}^{R_o} r^n \, dr$$

$$= \frac{N \eta_o \omega^n F(n,\Delta)}{n+1} (R_o^{n+1} - R_i^{n+1}) \qquad (22)$$

in which R_o and R_i are the outside and inside radii of the blades, respectively, and N is the number of blades. If the fluid parameters n and η_o are known, the torque and normal force values calculated from Equations (21) and (22) can be compared with experimental values as a check on the validity of the viscometric flow theory.

Another way of using the analysis is to determine viscosity functions from experimental torque and normal force results. A maximum shear rate, Γ_m, is defined:

$$\Gamma_m = \omega R_o/\Delta \qquad (23)$$

The maximum shear rate of Equation (23) is arbitrary since the velocity profile under the blade tip will never be exactly linear. However, insignificant error is introduced into the calculations by using the arbitrary definition. A viscosity corresponding to the maximum shear rate is obtained from the power law definition of Equation (2):

$$\eta_m = \eta_o \Gamma_m^{n-1} \qquad (24)$$

Equations (23) and (24) are substituted into Equations (21) and (22) to obtain the viscosity results:

$$\eta_m(\text{torque}) = \left(\frac{R_o}{\Delta}\right)^n \frac{T_p \, (n+2)}{(\omega R_o/\Delta) N D(n,\Delta)(R_o^{n+2} - R_i^{n+2})} \qquad (25)$$

$$\eta_m(\text{normal force}) = \left(\frac{R_o}{\Delta}\right)^n \frac{F_p \, (n+1)}{(\omega R_o/\Delta) N F(n,\Delta)(R_o^{n+1} - R_i^{n+1})} \qquad (26)$$

Unless the exponent n is known independently, the calculations will be of a trial and error nature. Strictly speaking this analysis can be valid only for constant exponent n over the shear rate range from zero to the maximum. If n is a weak function of shear rate it is probable that little error will result by using n corresponding to the maximum shear rate. If n is a strong function of shear rate it might be necessary to change the viscometric flow computer program to take this into account. In the coatings studied so far in this work, n has been seen to be a reasonably weak function of shear rate.

The Second Method of Analysis

The first step of the analysis is to reduce the data to tangential and normal force as functions of maximum velocity and gap, $D(V_o,\Delta)$ and $F(V_o,\Delta)$, respectively. As functions of variable velocity, these functions are defined as follows:

$$D(v,\Delta) = \text{tangential force (drag)/blade width} \tag{27}$$

$$F(v,\Delta) = \text{normal force/blade width} \tag{28}$$

Integrated torque and normal force are:

$$T_p = N \int_{R_i}^{R_o} D(v,\Delta)\, r\, dr \tag{29}$$

$$F_p = N \int_{R_i}^{R_o} F(v,\Delta)\, dr \tag{30}$$

in which N, R_o, and R_i are defined as before, and T_p and F_p are experimental torque and normal force values, respectively. A variable change from r to wear plate velocity is made as before, yielding:

$$r\,dr = v\,dv/\omega^2 = (R_o/V_o)^2\,v\,dv \tag{31}$$

in which V_o is again the velocity at R_o. Substitution into Equations (29) and (30) gives:

$$T_p = N(R_o/V_o)^2 \int_{V_i}^{V_o} D(v,\Delta)\,v\,dv \tag{32}$$

$$F_p = N(R_o/V_o) \int_{V_i}^{V_o} F(v,\Delta)\,dv \tag{33}$$

To isolate the D and F functions, Equations (32) and (33) are differentiated with respect to V_o, with Δ being constant:

$$\frac{d\,T_p}{d\,V_o} = -\frac{2\,T_p}{V_o} + N\left(\frac{R_o}{V_o}\right)^2 \left[D(V_o,\Delta)V_o - D(V_i,\Delta)V_i \frac{dV_i}{dV_o}\right] \tag{34}$$

$$\frac{d\,F_p}{d\,V_o} = -\frac{F_p}{V_o} + N\left(\frac{R_o}{V_o}\right)\left[F(V_o,\Delta) - F(V_i,\Delta)\frac{dV_i}{dV_o}\right] \tag{35}$$

in which V_i is the velocity at R_i. Since

$$dV_i/dV_o = V_i/V_o = R_i/R_o,$$

Equations (34) and (35) can be rearranged to give:

$$D(V_o,\Delta) - (R_i/R_o)^2\,D(V_i,\Delta) = \frac{2\,T_p}{NR_o^2}\left[1 + 1/2\,\frac{d\,\log(T_p)}{d\,\log(V_o)}\right] \tag{36}$$

$$F(V_o,\Delta) - (R_i/R_o)\,F(V_i,\Delta) = \frac{F_p}{NR_o}\left[1 + \frac{d\,\log(F_p)}{d\,\log(V_o)}\right] \tag{37}$$

Rapidly converging trial and error calculations will serve to determine the minor terms containing $D(V_i,\Delta)$ and $F(V_i,\Delta)$ in Equations (36) and (37). Not only will

these functions at V_i be less than the corresponding values at V_o, but the ratio R_i/R_o will also be much less than 1. At lower values of rotational speed, ω, the data will not extend down to V_i and an extrapolation will be required to eliminat these minor terms.

The functions $D(V_o,\Delta)$ and $F(V_o,\Delta)$ are comparable to drag and normal force results obtained with the Blade Nip Rheometer. The derivation of the functions does not depend on fluid properties or on flow behavior in the nips. However, it is assumed that drag and normal force are unique functions of gap and velocity. Thus, they would depend on the ratio ω/r but not on ω or r in any other way.

The second step in the analysis would be to use the derived drag and normal force functions to test a blade nip theory or to derive viscosity values. These applications have been documented in prior work (1,2).

DETERMINATION OF SECONDARY TORQUE CORRECTIONS

Low Gap Corrections

Secondary torque corrections are required for flow in the blades of the ring-blade geometry of Fig. 7 and for flow in the angle parts of the ring-angle geometries of Fig. 9 and 10. These are called low gap corrections since they decrease rapidly in magnitude with increasing gap, just as the primary torques do, and must be determined either from theory or from low gap experiments Blade corrections for the ring-blade geometry could be made experimentally by separate experiments with the blade geometry of Fig. 11, or by the application of a theory of nip flow and knowledge of the fluid properties. Since no data from this geometry are considered in this report, it will not be considered further.

For the ring-angle geometries, the corrections may be strictly theoretical or may be augmented with experimental results. At the simplest, if one assumes viscometric flow of a Newtonian fluid, the corrections would be unique functions of gap for a given geometry. This is illustrated in Fig. 12 for the geometry of Fig. 10. At low gaps such corrections would probably be satisfactory for all viscous fluids, since the values are reasonably low. In future work, when data analysis is put on a more routine basis, more accurate calculated values will be used which will reflect the non-Newtonian flow behavior. For viscoelastic coatings the calculated corrections of Fig. 12 are presumed to be inadequate. Future work may suggest theoretical corrections using a more sophisticated theory with experimentally determined fluid properties. Alternately, it may be desirable to use the ring-blade geometry, for which corrections can be determined experimentally, or the split ring geometry of Fig. 6, for which no corrections are required.

Large Gap Corrections

Secondary torque corrections, except for those previously discussed, are determined from large gap results (i.e., Δ = 0.15-0.6 cm). While the torque values at such large gaps result mainly from secondary flows, they also have contributions from the primary flows. Hence, it is desirable to estimate this primary contribution. In order to do this it is necessary that one have a known viscosity function and a theory describing flow in the primary regions, whether blades, ring-blade, or the ring-angle geometries are used. It is currently considered probable that viscometric flow theories will be satisfactory for all geometries. The greatest deviation from the theory is for highly viscoelastic coatings in blade flow and even these show relatively small deviations at low shear rates (i.e., large gaps) (1). If the experimentally determined

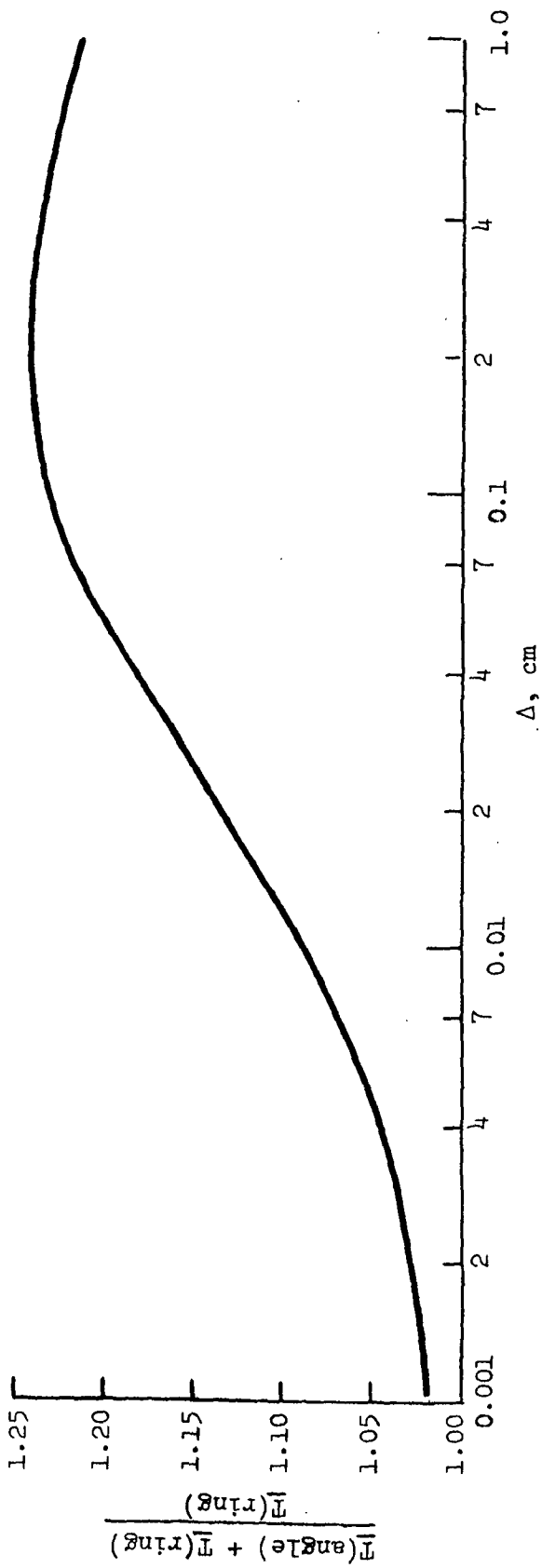

Figure 12. Relative Contributions to Torque by Angle and Primary Film for Newtonian Fluid. *Angle-Ring Geometry of Fig. 6*

viscosity function covers only the high shear rate range characteristic of the low gap results (0.001-0.01 cm), then an assumption is required concerning the extrapolation of the viscosity to low shear rate. For some fluids it may be desirable to obtain an estimate of low shear viscosity by some other means. A highly dilatant coating might be an example.

If an independent viscosity function is available in analyzing a set of data, then the determination of secondary torque is straightforward. If the secondary torque is to be used to correct primary data which are, in turn, to be used to determine the viscosity function, then a simple trial and error calculation will be required. The first trial would be to neglect the primary contribution to the wide gap results.

The secondary flows are complex and it is probably best to treat the resulting secondary torque empirically. An exception to the empiricism is made in order to estimate the small effect of translating the results from the wide gaps at which they are measured to the small gaps at which they are used. The exception is to assume that the major part of the torque results from shear between the wear plate and that area of the shear plate not covered by primary shearing surfaces. The film thickness involved, Δ_t, is the sum of the primary gap, Δ, and a large constant (the height of blades, rings, etc.). The change in Δ_t is moderate for the large change in Δ from wide to low gap, and it is assumed that the viscosity in this film is constant. This procedure results in plotting the secondary torque as a function of ω/Δ_t. Thus, when the secondary corrections are made, the appropriate value of Δ_t is used. It was found that this procedure generally tightened up the scatter of data from different large gap tests when compared to plots of torque *vs.* ω.

Secondary torque results for the ring-angle geometry are given in Fig. 13. Data were obtained using the "nonfloating" technique. The results for the PVA coating were not corrected for the primary flow contribution since there is a high probability that the experimentally determined viscosity funct is in considerable error. The absence of corrections for primary flow probabl accounts for the lower gap results having larger torque values than those of the larger gaps. The deviation of the open circles at the low end of the star data is probably caused by drift in the zero torque setting. Data were not obtained at the larger gaps and the highest speeds because of an apparent flow instability. This may be due to a partial voiding of the flow region between the shear plate and the wear plate.

In Fig. 14 results of secondary torque vs. ω/Δ_t are presented for the blade geometry. The data for the coatings were obtained using the "floating" technique, while for the glycerin solution the "nonfloating" technique was used It is apparent from the figure that the latter technique is the more desirable when obtaining torque data, even though the first technique may be required in order to obtain secondary normal force data. Again, the PVA data were not corrected for the primary flow contributions and the low gap values again exhibit higher torques than those of the large gaps.

A comparison of secondary torque results for the two geometries is given by the dashed lines in Fig. 14. With this limited amount of data, it is perhaps best not to make too much of the comparison, except to comment that some comfort is to be taken from the fact that the two sets of data are comparat in magnitude.

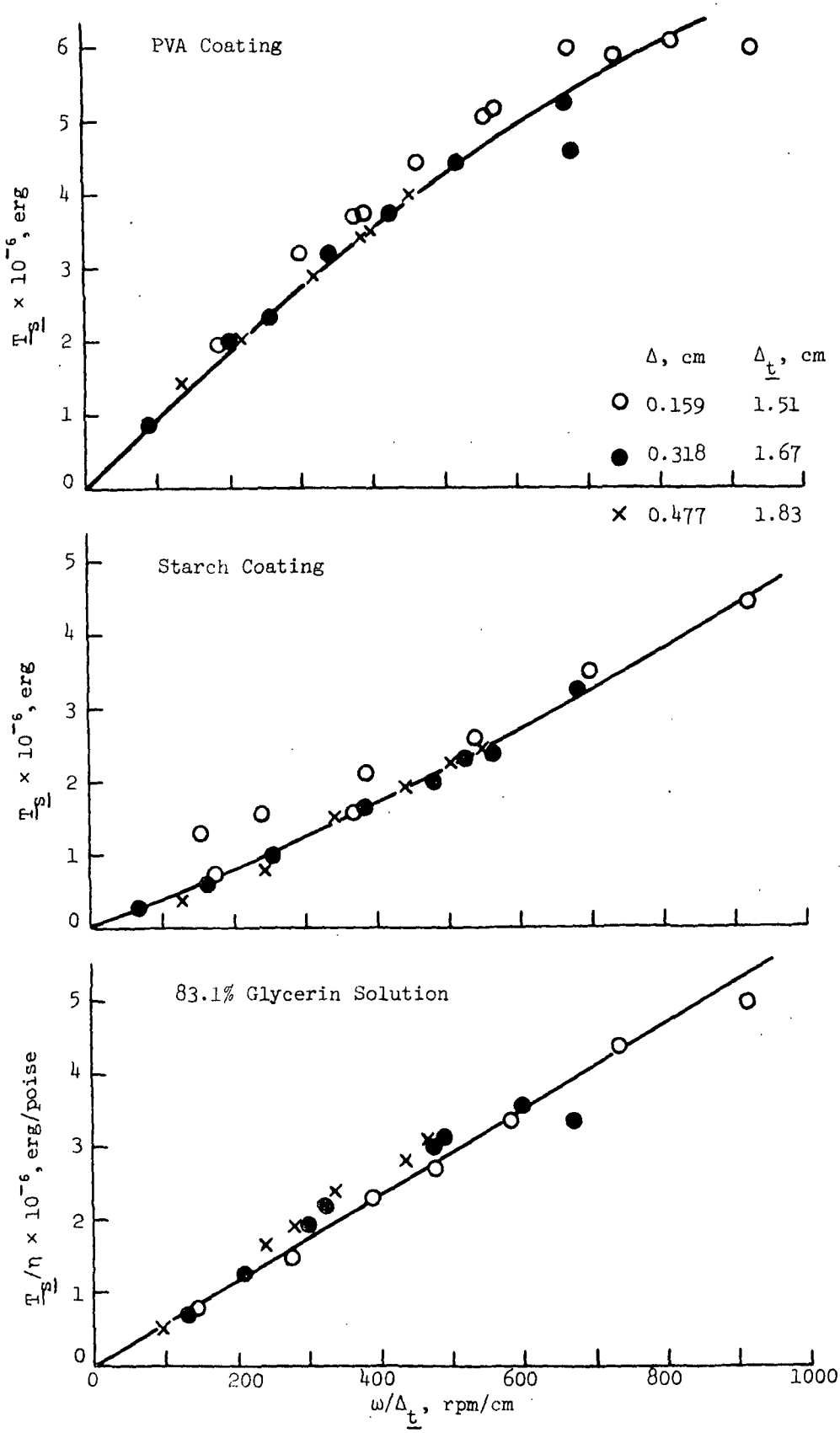

Figure 13. Secondary Torque for the Ring-Angle Shear Plate Geometry

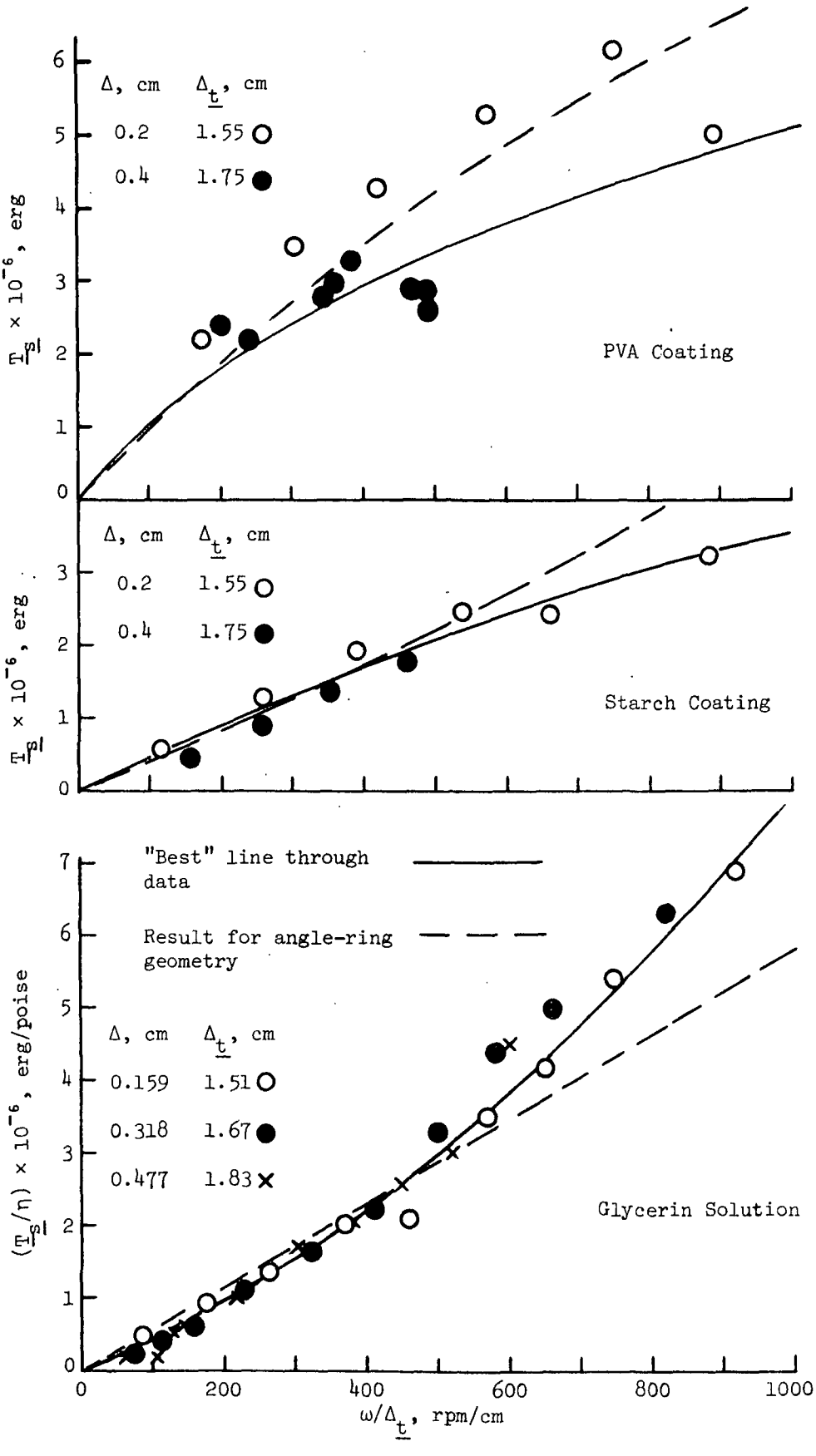

Figure 14. Secondary Torque for the Blade Shear Plate Geometry

Some examples of the magnitude of the secondary flow corrections, with and without the primary contributions to the secondary flows, are given in Tables II, III, and IV. Certain important conclusions may be drawn from these results:

1) In all cases the secondary torque corrections are significant and in some cases dominate the raw torque measurements.

2) The primary contribution to the secondary torque corrections is generally quite small, but over some ranges of variables, they cannot be neglected.

3) There is probably an upper limit to the gap for obtaining useful data. This may be of the order of 0.01 cm.

TABLE II

EXAMPLES OF SECONDARY TORQUE CORRECTIONS:
GLYCERIN SOLUTION, BLADE GEOMETRY

Δ, cm	$\underline{T}$, erg[a]	$\underline{T}_p$, erg[b]	$\underline{T}_p$, erg[c]
	ω = 202 rpm		
0.68×10^{-3}	6.0×10^{6}	5.6×10^{6}	5.6×10^{6}
3.54	2.50	2.00	2.06
8.8	1.54	1.04	1.10
	ω = 1406 rpm		
2.22	22.7	16.4	17.4
7.7	13.1	7.0	8.0
10.4	11.8	5.5	6.5
16.4	9.5	3.2	4.2
26.6	7.6	1.3	2.3

[a] Total measured torque.
[b] Total torque corrected for secondary torque. Secondary torque not adjusted for primary torque contribution.
[c] Corrected total torque. Secondary torque adjusted for primary torque contribution.

TABLE III

EXAMPLES OF SECONDARY TORQUE CORRECTIONS:
GLYCERIN SOLUTION, ANGLE-RING GEOMETRY

Δ, cm	$\underline{T}$, erg[a]	$\underline{T}_p$, erg[b]	$\underline{T}_p$, erg[c]
	ω = 300 rpm		
2.66×10^{-3}	6.8×10^{6}	6.0×10^{6}	6.1×10^{6}
4.7	4.37	3.53	3.61
7.2	3.32	2.49	2.57
	ω = 1390 rpm		
4.8	18.3	14.5	14.9
9.5	11.8	8.0	8.4
15.0	9.3	5.6	5.9

[a]Total measured torque.
[b]Total torque corrected for secondary torque. Secondary torque not adjusted for primary torque contribution.
[c]Corrected total torque. Secondary torque adjusted for primary torque contribution.

TABLE IV

EXAMPLES OF SECONDARY TORQUE CORRECTIONS:
STARCH COATING, ANGLE-RING GEOMETRY

Δ, cm	ω, rpm	$\underline{T}$, erg[a]	$\underline{T}_p$, erg[b]	$\underline{T}_p$, erg[c]
		$\underline{F}$ ∿17 lb		
2.28×10^{-3}	204	4.1×10^{6}	3.4×10^{6}	3.5×10^{6}
4.7	950	9.9	6.3	6.7
7.6	1400	11.3	5.3	6.1
		$\underline{F}$ ∿27 lb		
1.93	238	5.0	4.2	4.3
4.05	1380	13.9	8.0	8.8
		$\underline{F}$ ∿47 lb		
1.56	264	6.0	5.1	5.2
2.97	1390	16.1	10.2	10.9

[a]Total measured torque.
[b]Total torque corrected for secondary torque. Secondary torque not adjusted for primary torque contribution.
[c]Corrected total torque. Secondary torque adjusted for primary torque contribution.

SECONDARY NORMAL FORCE CORRECTIONS FOR BLADES

Wide gap normal force measurements were made on the two coatings in order to determine the magnitude of the secondary normal force corrections. The primary force adjustments were made assuming that the blade flow is viscometric. The results are presented in Tables V and VI. It was believed that there would be negligible contributions by viscoelastic normal stresses to the corrections, since the normal stresses fall off very rapidly with decreasing shear rate. This leaves angular momentum as the major contribution to the normal force corrections. It is apparent from the results that the secondary corrections are much less than predicted, and, in fact, seem to be little more than random error. The reason may be that radial flows can relieve the momentum tension at the center because of the wide flow channels available. The degree of random scatter in the results is probably due to frictional contact on the guide posts. The best procedure to follow in making such future corrections may be to assume a linear relationship between ω and $\underline{F_s}$.

TABLE V

SECONDARY NORMAL FORCE CORRECTIONS,
STARCH COATING, BLADE GEOMETRY

ω, rpm	$\underline{F}$, lb[a]	$\underline{F}_p$, lb[b]	$\underline{F}_s$, lb[c]	$\underline{F}_s$, lb (pred.)[d]
		Δ = 0.2 cm		
178	1.2	0.2	1.0	-0.8
400	0.9	0.4	0.5	-3.1
606	1.2	0.5	0.7	-7.2
836	1.0	0.6	0.4	-13.6
1024	-1.3	0.7	-2.0	-20.5
1366	-0.1	0.9	-1.0	-37
		Δ = 0.4 cm		
272	-1.8	0.1	-1.9	-1.4
444	-1.1	0.1	-1.2	-3.8
616	-1.0	0.1	-1.1	-7.4
808	-1.0	0.1	-1.1	-12.7

[a] Measured normal force.
[b] Primary force adjustment.
[c] Secondary normal force correction.
[d] Secondary normal force correction predicted by Equation (1), with ρ = 1.5 g/cm^3 and $\underline{R}$ = 6.7 cm.

TABLE VI

SECONDARY NORMAL FORCE CORRECTIONS,
PVA COATING, BLADE GEOMETRY

ω, rpm	$\underline{F}$, lb[a]	$\underline{F}_p$, lb[b]	$\underline{F}_s$, lb[c]	$\underline{F}_s$, lb (pred.)[d]
		Δ = 0.2 cm		
270	0.0	0.4	-0.4	-1.4
470	-0.3	0.6	-0.9	-4.3
650	-0.2	0.7	-0.9	-8.3
880	-1.3	0.9	-2.2	-15.2
1160	-1.7	1.0	-2.7	-26.0
1380	-1.0	1.2	-2.2	-37.0
		Δ = 0.4 cm		
350	-0.6	0.1	-0.7	-2.4
420	-1.3	0.1	-1.4	-3.4
600	-1.0	0.1	-1.1	-7.0
630	-1.2	0.1	-1.3	-7.8
670	-1.1	0.1	-1.2	-8.8
830	-1.2	0.2	-1.4	-13.5
850	-1.2	0.2	-1.4	-14.0
850	-0.9	0.2	-1.1	-14.0

[a] Measured normal force.
[b] Primary force adjustment.
[c] Secondary normal force correction.
[d] Secondary normal force correction predicted by Equation (1), with ρ = 1.5 g/cm^3 and $\underline{R}$ = 6.7 cm.

EXPERIMENTAL RESULTS

NEWTONIAN FLUID

Experimental Conditions

The test fluid was an 83.1% solution of industrial grade glycerin in water. The solution concentration was determined from Cannon-Fenske viscosity measurements.

Rheometer measurements were made using the ring-angle geometry shown in Fig. 10 and the blade geometry shown in Fig. 11.

Results Obtained with the Ring-Angle Geometry

In Fig. 15, experimental values of normal force are compared with values predicted for viscometric flow. Viscometric flow predictions were obtained using a computer program developed in prior work (1). In a previous discussion of the tilt phenomenon it was mentioned that normal force values are generally much greater than would be expected, and these results illustrate this fact. It should be emphasized that these results in themselves would not confirm such anomolous behavior since there are no independent measurements proving that one could expect results to conform to viscometric flow theory in the ring-angle geometry. The tilt phenomenon was deduced from an earlier experiment with the ring-blade geometry in which independent blade measurements were available. However, it is presumed that the flow should be approximately viscometric and that the results in Fig. 15 at least indicate the order of magnitude deviation caused by tilt. It is apparent from the results that the film thickness was generally much greater than expected and this accounts for the lower than expected maximum shear rate obtained.

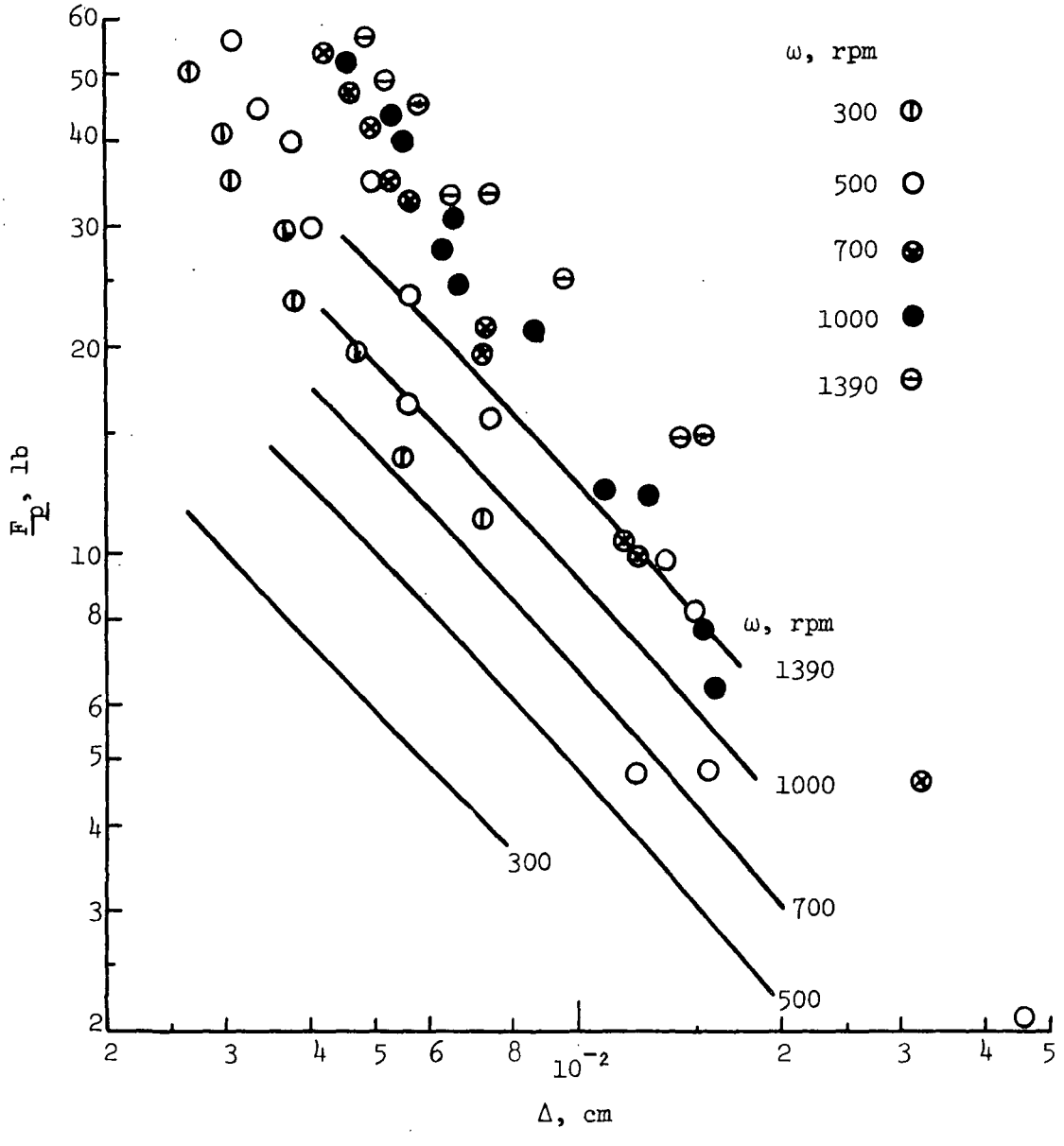

Figure 15. Comparison of Experimental (Points) and Theoretical (Lines) Normal Force, 83.1% Glycerin Solution, Ring-Angle Geometry (Fig. 10), Expt. 41

The torque results are presented in Table VII. The following conclusions are drawn from the results.

1) With gap (Δ) values below about 10^{-2} cm, reasonably good measurements of the viscosity are made at all rotational speeds.

TABLE VII

EXPERIMENTAL TORQUE RESULTS ON 83.1% GLYCERIN SOLUTION, RING-ANGLE GEOMETRY EXPT. 41

Expt. Order	Δ, cm	Γ(max.), sec^{-1}	η(exp.), poise	η(true), poise	T_s/T^a
		Run 4, ω = 300 rpm			
4	2.66×10^{-3}	7.9×10^{4}	0.54	0.60	0.11
5	2.99	7.0	0.55	0.60	0.12
3	3.07	6.8	0.55	0.60	0.12
6	3.70	5.7	0.58	0.61	0.14
2	3.8	5.5	0.56	0.60	0.15
7	4.7	4.5	0.57	0.61	0.17
1	5.5	3.81	0.57	0.60	0.19
8	7.2	2.91	0.62	0.61	0.23
		Runs 1 & 2, ω = 500 rpm			
5	3.10×10^{-3}	1.13×10^{5}	0.57	0.61	0.13
4	3.38	1.04	0.56	0.61	0.14
6	3.75	9.3×10^{4}	0.57	0.61	0.15
3	4.05	8.6	0.57	0.61	0.16
7	5.0	7.0	0.61	0.61	0.18
2	5.6	6.2	0.58	0.61	0.20
1	5.7	6.1	0.72	0.61	0.17
8	7.1	4.9	0.57	0.61	0.24
16	7.4	4.7	0.62	0.60	0.23
9	12.1	2.89	0.62	0.61	0.32
13	13.6	2.57	1.34	0.60	0.20
14	15.6	2.24	1.08	0.60	0.26
15	22.0	1.57	1.48	0.60	0.27
10	46	7.6×10^{3}	0.48	0.61	0.69
11	91	3.84	--	0.61	1.03
12	94	3.72	0.04	0.61	0.98

[a] See end of table for footnote.

TABLE VII (Continued)

EXPERIMENTAL TORQUE RESULTS ON 83.1% GLYCERIN SOLUTION,
RING-ANGLE GEOMETRY EXPT. 41

Expt. Order	Δ, cm	Γ(max.), sec^{-1}	η(exp.), poise	η(true), poise	T_s/T^a
		Run 5, ω = 700 rpm			
4	4.2×10^{-3}	1.17×10^{5}	0.64	0.62	0.14
3	4.6	1.06	0.67	0.62	0.15
5	4.9	1.00	0.65	0.62	0.16
2	5.1	9.6×10^{4}	0.65	0.62	0.17
6	5.6	8.8	0.65	0.61	0.18
1	7.2	6.8	0.65	0.62	0.22
7	7.3	6.7	0.69	0.62	0.21
8	11.7	4.2	0.76	0.62	0.27
9	11.9	4.1	0.71	0.62	0.29
10	32.3	1.51	0.77	0.62	0.50
		Run 3, ω = 1000 rpm			
5	4.5×10^{-3}	1.55×10^{5}	0.53	0.58	0.17
4	4.9	1.43	0.56	0.59	0.17
6	5.5	1.27	0.58	0.58	0.18
11	6.3	1.11	0.55	0.57	0.21
7	6.5	1.08	0.55	0.58	0.21
3	6.6	1.06	0.57	0.59	0.21
8	8.6	8.1×10^{4}	0.58	0.57	0.26
1	11.0	6.4	0.61	0.59	0.29
9	12.8	5.5	0.65	0.57	0.31
2	15.3	4.6	0.63	0.59	0.36
10	16.0	4.4	0.70	0.57	0.34

[a]See end of table for footnote.

TABLE VII (Continued)

EXPERIMENTAL TORQUE RESULTS ON 83.1% GLYCERIN SOLUTION, RING-ANGLE GEOMETRY EXPT 41

Expt. Order	Δ, cm	Γ(max.), sec^{-1}	η(exp.), poise	η(true), poise	T_s/T^a
		Run 6, ω = 1390 rpm			
4	4.8×10^{-3}	2.02×10^{5}	0.51	0.59	0.19
3	5.2	1.87	0.51	0.60	0.20
5	5.8	1.68	0.52	0.58	0.21
2	6.4	1.52	0.55	0.61	0.22
6	7.4	1.31	0.53	0.58	0.25
7	9.5	1.02	0.55	0.57	0.29
1	14.2	6.9×10^{4}	0.66	0.61	0.33
8	15.0	6.5	0.60	0.57	0.36

[a]This is the fraction of the total torque which is "secondary."

2) As Δ increases above about 10^{-2} cm, deviations from theory are greater than can be accounted for by secondary torque corrections, which are indicated in the last column as fractions of the measured values. It is presumed that the deviations are caused by the tilt effect and that there is a practical upper limit of about 10^{-2} cm for gap, at least for this geometry.

3) It will be noted that the experimental viscosities for the maximum speed, ω = 1390 rpm, were generally lower than the other values. It is possible that this is due to viscous heating since no attempt was made to correct the results except for the corrections made for the rise in bulk temperature. The evident absence of major viscous heating effects in these results is very encouraging since glycerin viscosity is much more temperature sensitive than any coatings tested in this project.

4) During this experiment, the speed was set for each run at the beginning and entered in the notebook but not recorded on the data chart. This was done to reduce the actual running time for each data set, from that time required to record four values to three values. This is now considered bad practice for two reasons: a mistake in recording ω cannot be checked later on the chart; and it presumes a constant speed which has been found to be only approximately valid in some cases. In other experiments ω was recorded for each data set. An error in ω could account for the experimental viscosity being generally larger for ω = 700 rpm, than that obtained at lower and higher speeds.

Results Obtained with the Blade Geometry

Torque and normal force results are presented in Fig. 16 and 17, respectively. The lines are predictions made by assuming viscometric flow. The results are uncorrected for viscous heating except for the apparent change in true fluid viscosity with change in bulk temperature of the fluid. The results are considered in three respects: the reproducibility of the data within and between runs, comparison with previous results obtained using the Blade Nip Rheometer, and the conformity of the results with predictions made assuming viscometric flow.

Data within runs were taken in random order and, considering the small scatter in the points, the error within runs appears to be quite low. The duplication of results with repeat runs suggests low random error between runs as well. It may be desirable later to take more extensive data on glycerin, or coatings, in order to make a quantitative error analysis.

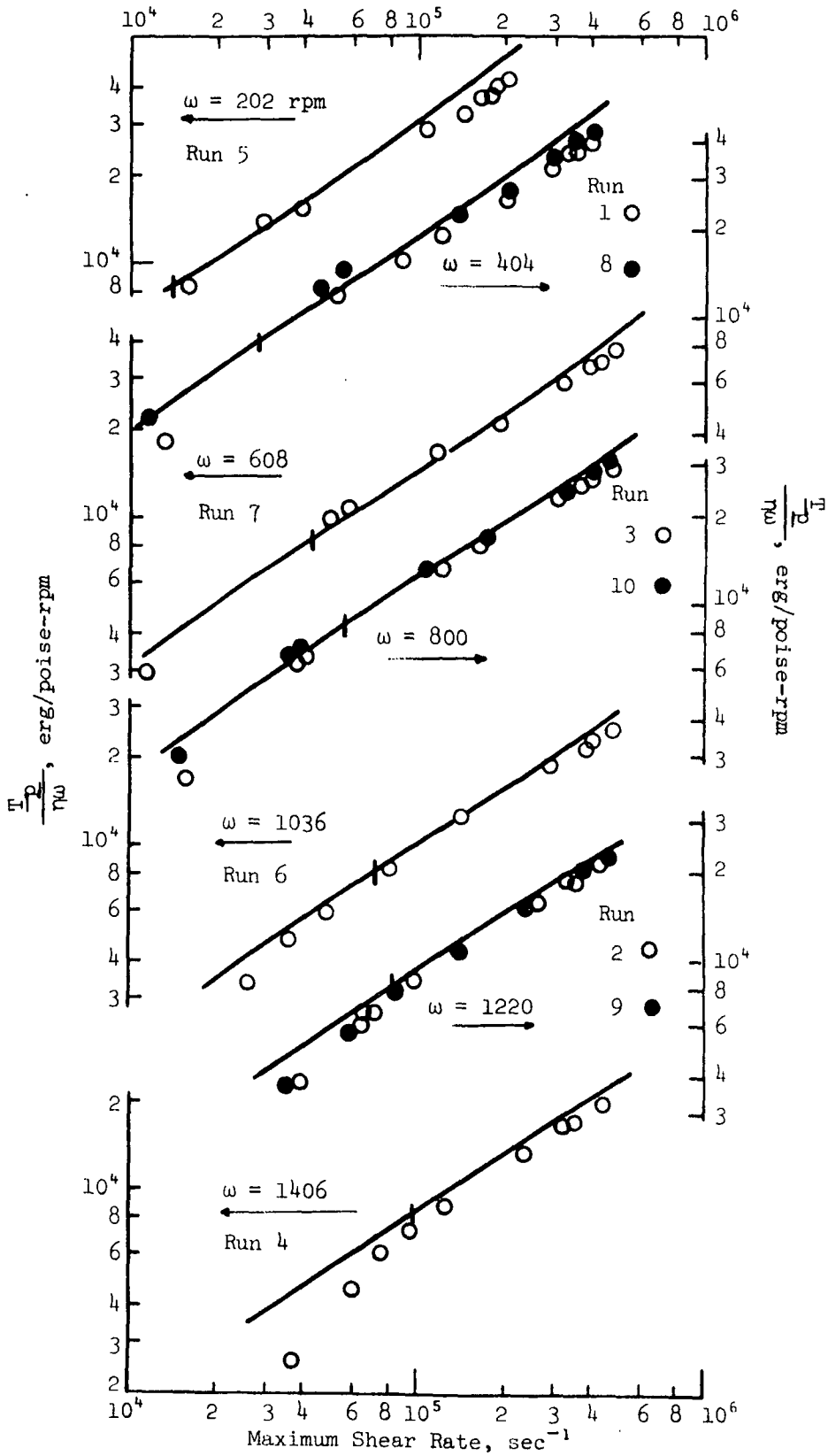

Figure 16. Blade Geometry Torque Results for 83.1% Glycerin Solution (Approximate Viscosity = 0.65 Poise), Expt. 35. The Lines are Theoretical Predictions for Viscometric Flow

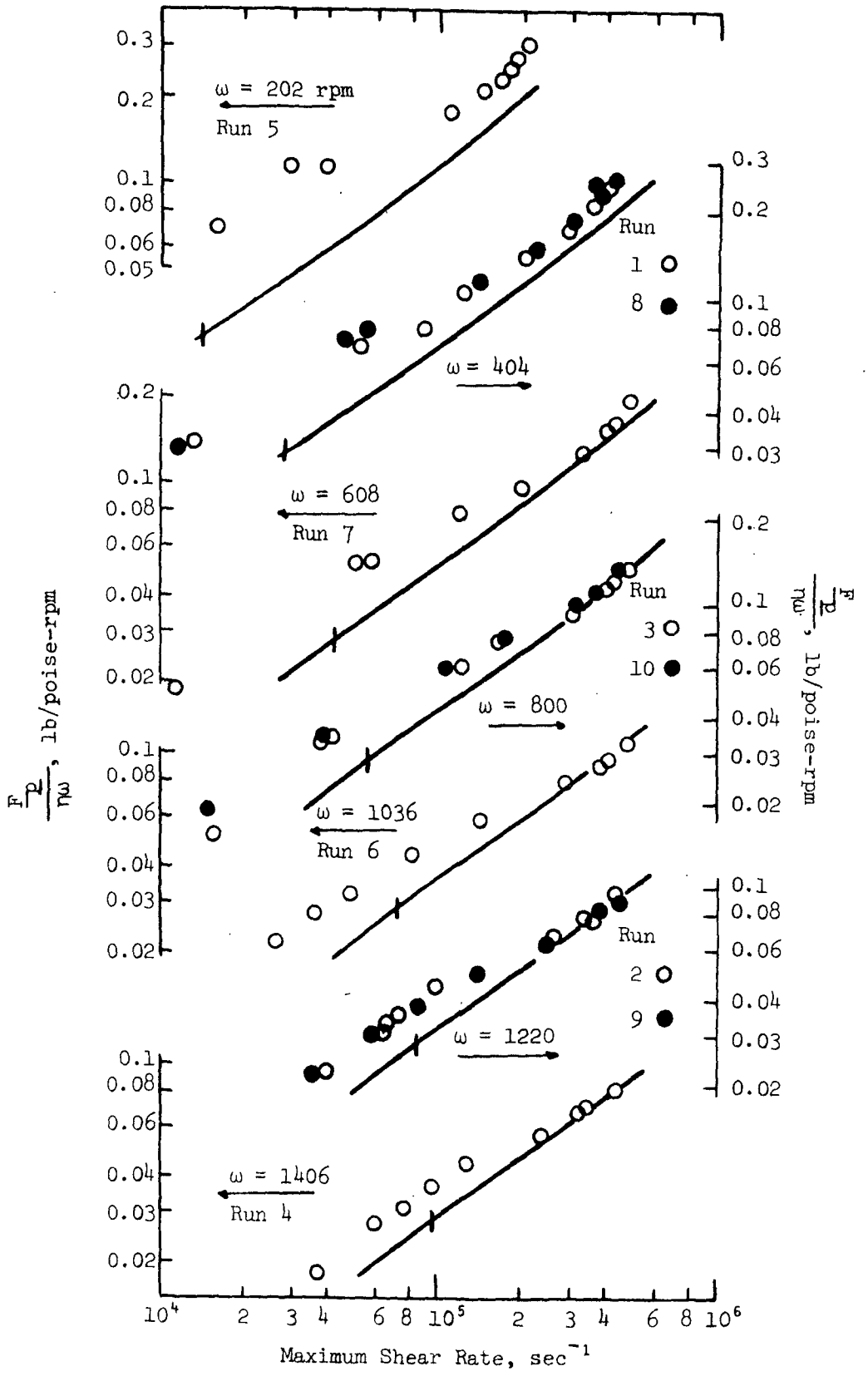

Figure 17. Blade Geometry Normal Force Results for 83.1% Glycerin Solution (Approximate Viscosity = 0.65 Poise), Expt. 35. The Lines are Theoretical Predictions for Viscometric Flow

The only fair comparison which can be made with Blade Nip Rheometer results is to compare the present results obtained at the three highest speeds ($\omega \geq 1036$ rpm) with those results given for a Newtonian viscosity of 0.6 poise in Fig. 13, Ref. (1). The comparison indicates similar results obtained in the two cases. Considering the differences in the test instruments, and the fact that the present data were not corrected for viscous heating, this is encouraging. A better comparison could be made if the present results extended to higher shear rates, where a drastic drop in drag viscosity was found previously. Using the present blade geometry, it will be necessary to test a lower viscosity glycerin solution in order to obtain comparable high shear rate results.

The torque results conform quite well to the theory, except at the higher ω, where deviations occur at low shear rates. The normal force results show less conformity, especially at the lower speeds. Application of the revised theory may indicate whether these deviations are because of inadequacies in the viscometric theory or experimental abberations. The normal force results at the lower speeds suggest the latter since all factors which would be expected to cause deviations from the theory are absent: large inertial forces, angular momentum forces, turbulence, etc.

VISCOUS COATING

Experimental Conditions

The formulation of the coating was:

KCS (S.D.) clay:	100 parts
Stayco M starch:	20 parts
Quadrafos:	0.1 part
% solids = 51.3	

The clay slurry was mixed for 30 minutes at 75% solids using a Hobart mixer. Mixing was done with a wire whip at low speed (No. 1), and these conditions were used throughout. The slurry was then diluted to 71% solids and mixed for 20 minutes. The starch was cooked for five minutes using steam at 22.0% solids. The starch was then mixed with the clay slip in the Hobart for 30 minutes.

Rheometer measurements were made using the ring-angle geometry shown in Fig. 10 and the blade geometry shown in Fig. 11.

Results Obtained with the Ring-Angle Geometry

Corrections for the torque contribution of the angle part of the geometry were made using the Newtonian predictions given in Fig. 12. The actual corrections would be a little larger for a power law exponent less than one, but, since the corrections are small (of the order of 7%) it was considered satisfactory to use them as is.

The results are presented in Fig. 18. The scatter of the data is quite low and the same viscosity function is obtained with different normal force values. The single low point (Run 1) was the first data obtained and may be low because insufficient time was allowed for the machine to reach steady state temperature in all parts. It is unlikely that this could be a result of thixotropic breakdown since the shearing time was only about 6 sec for each set of recordings, and the energy input is to 900 ml of test fluid. Since reliable measures of viscosity were obtained for the Newtonian fluid and the scatter of the data here is low, these results are also considered to be a reliable measure of the coating viscosity.

Extrapolation of the results to the Hercules range seem to indicate larger viscosities due to less thixotropic breakdown. This is uncertain,

however, because of such meagre amount of data as well as the long extrapolation involved.

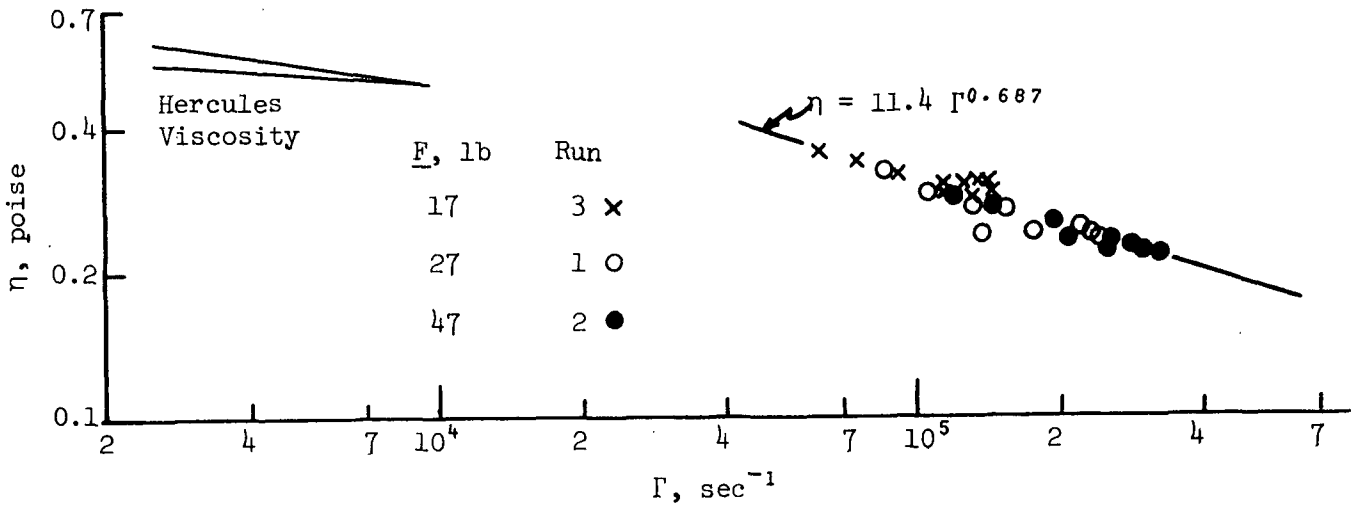

Figure 18. Ring-Angle Results for Viscous (Starch) Coating

Results Obtained with the Blade Geometry

Torque and normal force data are presented in Fig. 19. Best fit lines are drawn through the data and have no theoretical significance. Since data within runs were obtained in random order, the relatively low scatter indicates low random error within runs. Duplicate runs were made at 400 rpm (Runs 1 and 6). There is some evidence of a change in torque but very little for normal force. The former could be due to thixotropic breakdown since the second of the two runs followed the run at maximum speed (i.e., maximum energy input into the coating). More extensive data will be required to clarify this point, however.

The ring-angle power law exponent determined with ring-angle results, 0.687, was used with viscometric flow theory to obtain viscosity predictions for the blade geometry results. The results are given in Fig. 20. The deviations of these results from the "true" viscosity (determined with the ring-angle geometry) is much larger than expected in light of the Newtonian results.

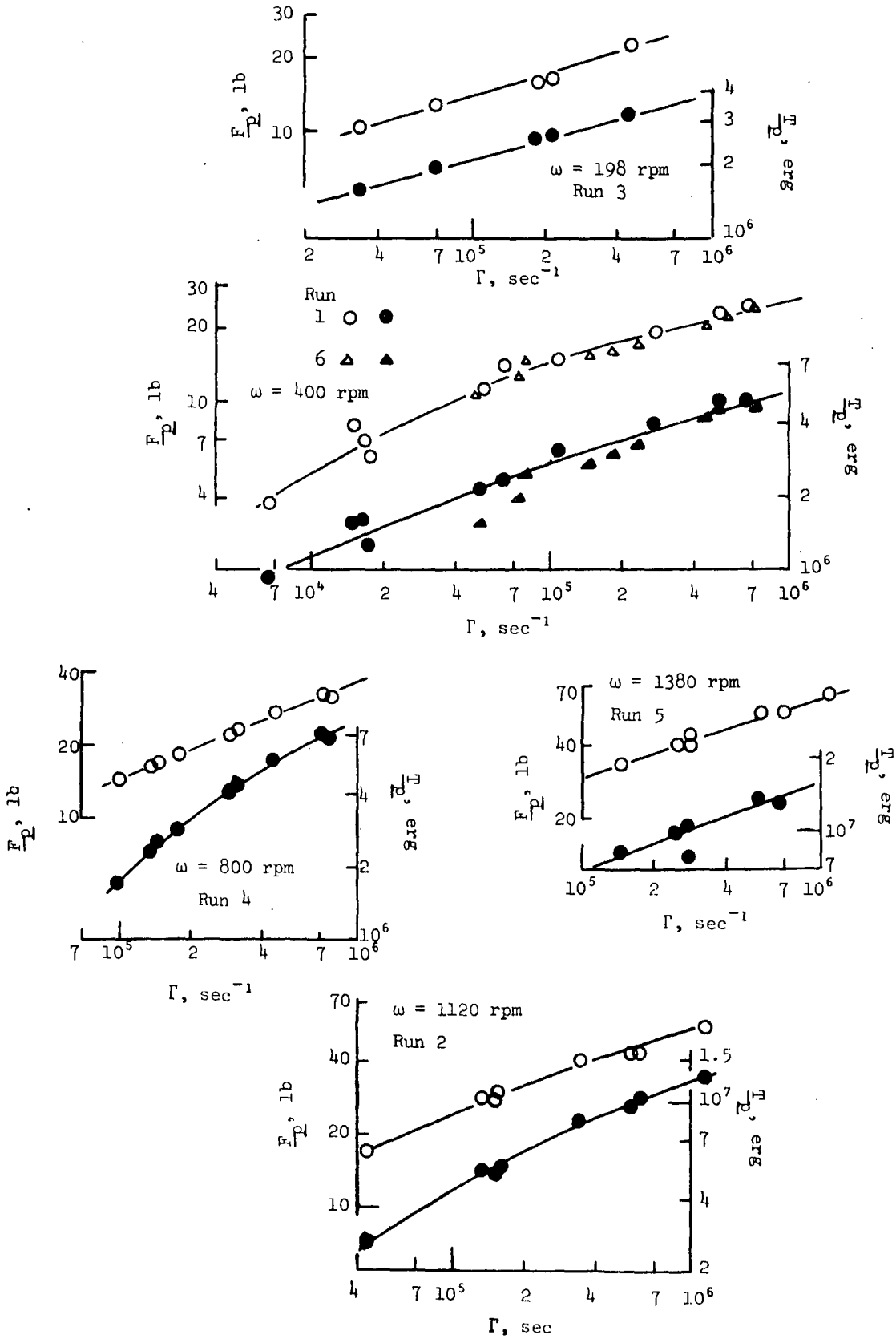

Figure 19. Torque and Normal Force Data for Starch Coating, Blade Geometry, Expt. 42

Some duplicate experiments will have to be performed in order to determine i
these deviations are real, or if some unexplained experimental difficulty exi

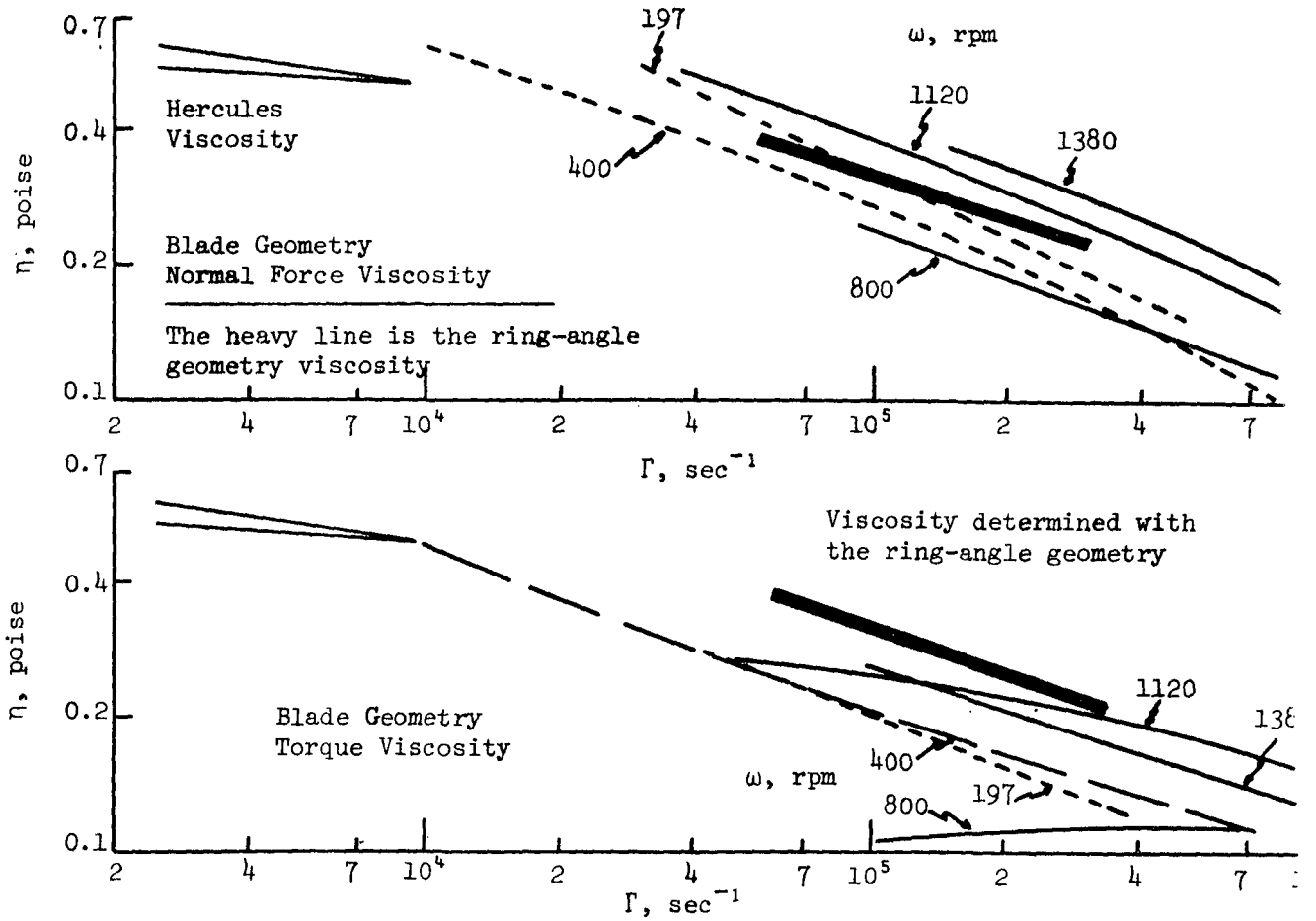

Figure 20. Various Experimental Measures of Viscosity for the Starch Coating, Expt. 42

In Fig. 21 the high speed blade results and the ring-angle results are compared with Blade Nip Rheometer results previously reported [Fig. 18, Ref. (1)]. The latter results are shifted on the η axis so that the Hercules results are the same for the different coatings. An interesting observation may be made by comparing the different results: the ring-angle results are presumably the true viscosity with little thixotropic breakdown. The Blade Nip Rheometer results also have low thixotropic breakdown and conform to the

true viscosity in the common shear rate range. At low shear rates the blade results show a larger viscosity than that obtained with the Hercules viscometer. This is evidence supporting the contention that blade nip measurements give more meaningful measurements of viscosity than conventional viscometers since they do not reflect large thixotropic breakdown.

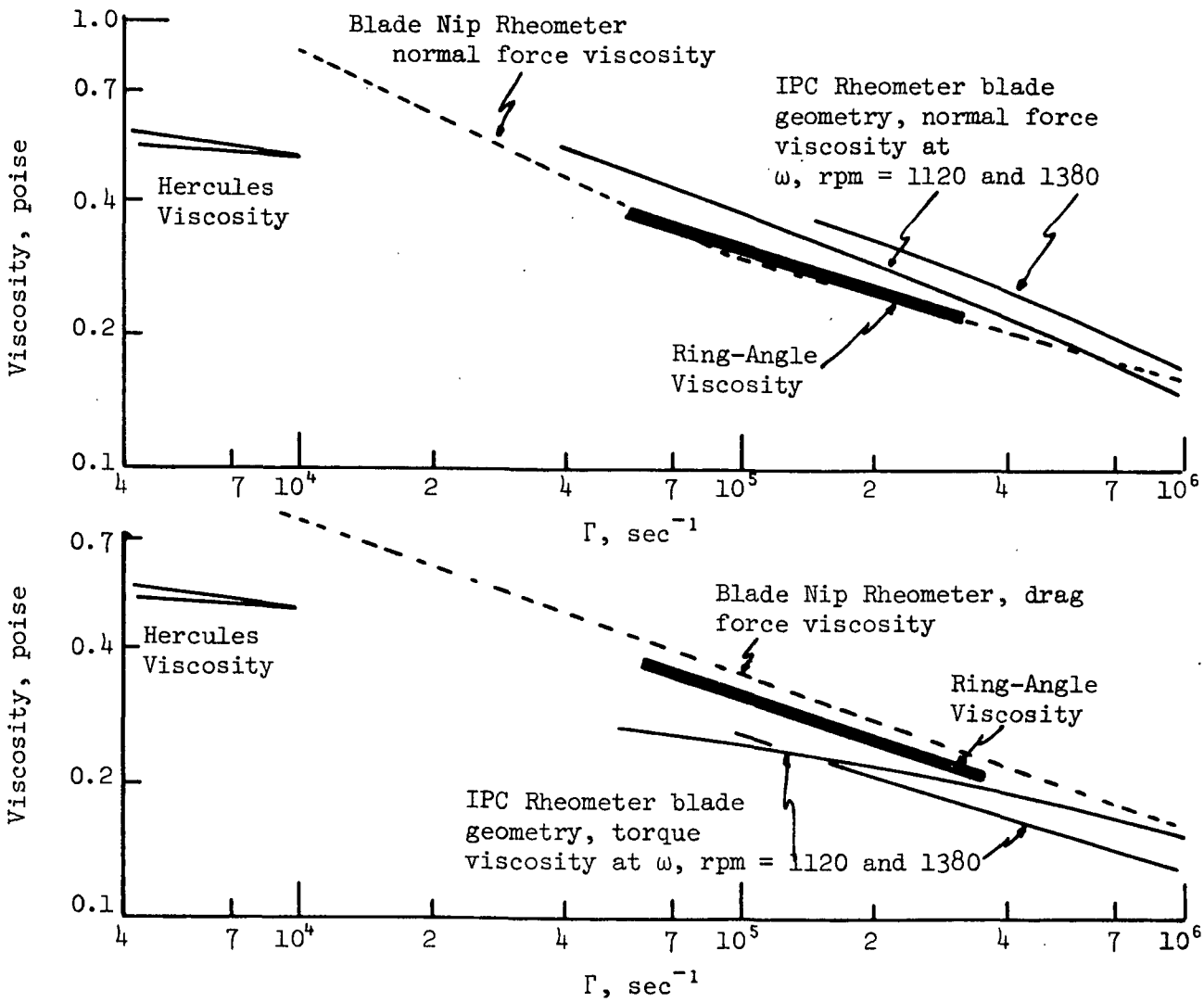

Figure 21. Comparison of Starch Coating Viscosity Determined by the IPC Rheometer, Blade and Ring-Angle Geometries, the Blade Nip Rheometer, and the Hercules Viscometer, Expt. 42

VISCOELASTIC COATING

Experimental Conditions

The coating formulation was as follows:

KCS (S.D.) clay:	100 parts
Du Pont Elvanol polyvinyl alcohol (PVA)	5 parts
Quadrafos:	0.1 part
% solids: 50.0	

The clay slip was prepared as indicated previously for the starch coating. The PVA was dissolved in water at 90°C while stirring for 15 minutes. The PVA solution was 7.23% solids. After cooling, the solution was added to the clay slip in the Hobart mixer. To avoid shock, the addition was done very slowly while mixing. After all the PVA was added, the coating was mixed for an additional 30 minutes.

Rheometer measurements were made using the ring-angle geometry shown in Fig. 10 and the blade geometry shown in Fig. 11.

Results Obtained with the Ring-Angle Geometry

The tangential force caused by viscoelastic fluids in blade doctoring has been seen to be much greater than predicted for viscometric flow for blade angles of 10° (1) and for 45° (2). It is, thus, expected that the angle effect for the 20° angles in the ring-angle geometry would be much greater than predicted by viscometric theory, especially as the shear rate exceeds 10^5 sec^{-1}. Due to uncertainty concerning the magnitude of the corrections, the results presented in Fig. 22 for the ring-angle geometry have not been corrected for this angle effect. The effect of such a correction would probably be to lower

the points about 10% at the low shear rate end and considerably more at the high shear rate. If this geometry is to be used for future viscosity measurements, there must be some convincing basis for making a correction. More likely it will be advantageous to use the ring blade or the split ring geometry for such fluids. The results, as presented, probably give an order of magnitude estimate of the viscosity, with the most reliable results being in the low shear rate part.

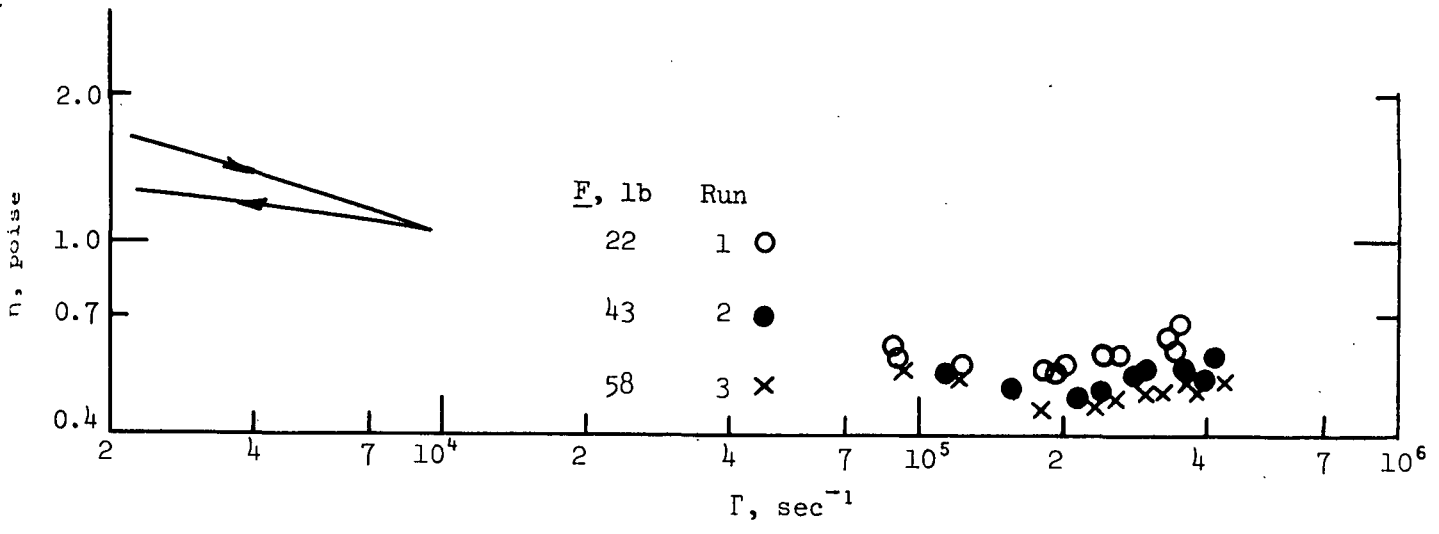

Figure 22. PVA Coating Viscosity Estimated from Ring-Angle Data, Expt. 42

Results Obtained with the Blade Geometry

The corrected torque and normal force results are plotted in Fig. 23 as functions of the maximum shear rate. There appears to be little random error within runs. As before, the data were taken in random order. The relatively large scatter of normal force values at low shear rates for Run 3 (top set of data) may indicate that a minimum threshold exists in the normal force of about 20 lb, below which useful data cannot be obtained. Best fit lines were drawn through the data and have no theoretical significance.

Viscosity values were calculated from these results assuming viscometric flow. The values are presented in Fig. 24. It was not expected that

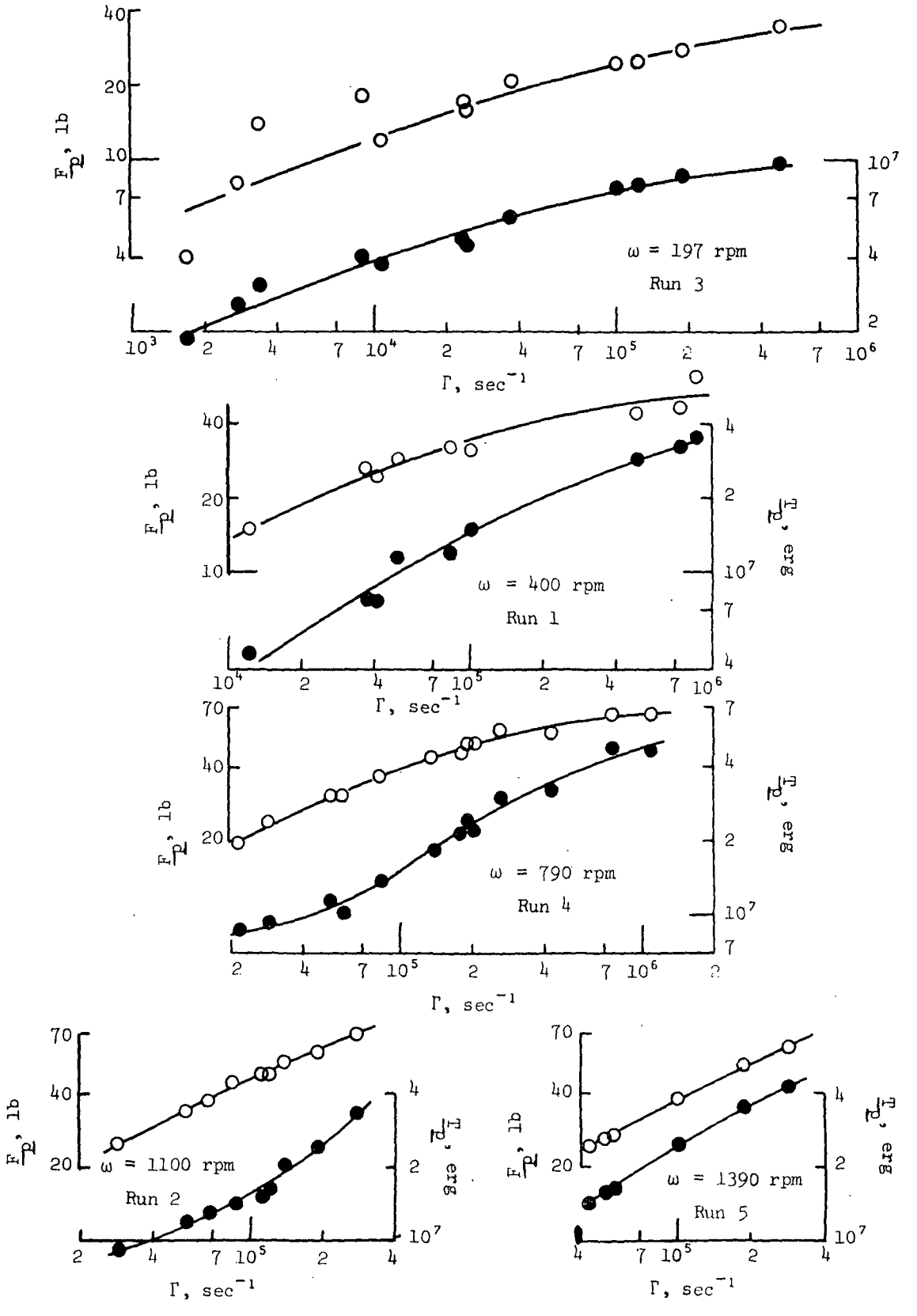

Figure 23. Torque and Normal Force Data for PVA Coating, Blade Geometry, Expt. 42

these results would conform to viscometric theory, but the analysis was made to compare them with those results obtained previously with 10° blades using the Blade Nip Rheometer [i.e., see results for Fluid 21, Fig. 20B, Ref. (1)]. Examining the results for the highest speed in Fig. 24, with the previous results, it appears that the viscoelastic effect is present here but less pronounced. The increase over the theory is much greater for torques than normal force as noted earlier, but the increase to a maximum viscosity is not observed. Two other observations may be pertinent; the results for various speeds appear to converge at low shear rates, see also in prior work, and there is some indication that the viscosities at the lowest speeds may approximate the true viscosity.

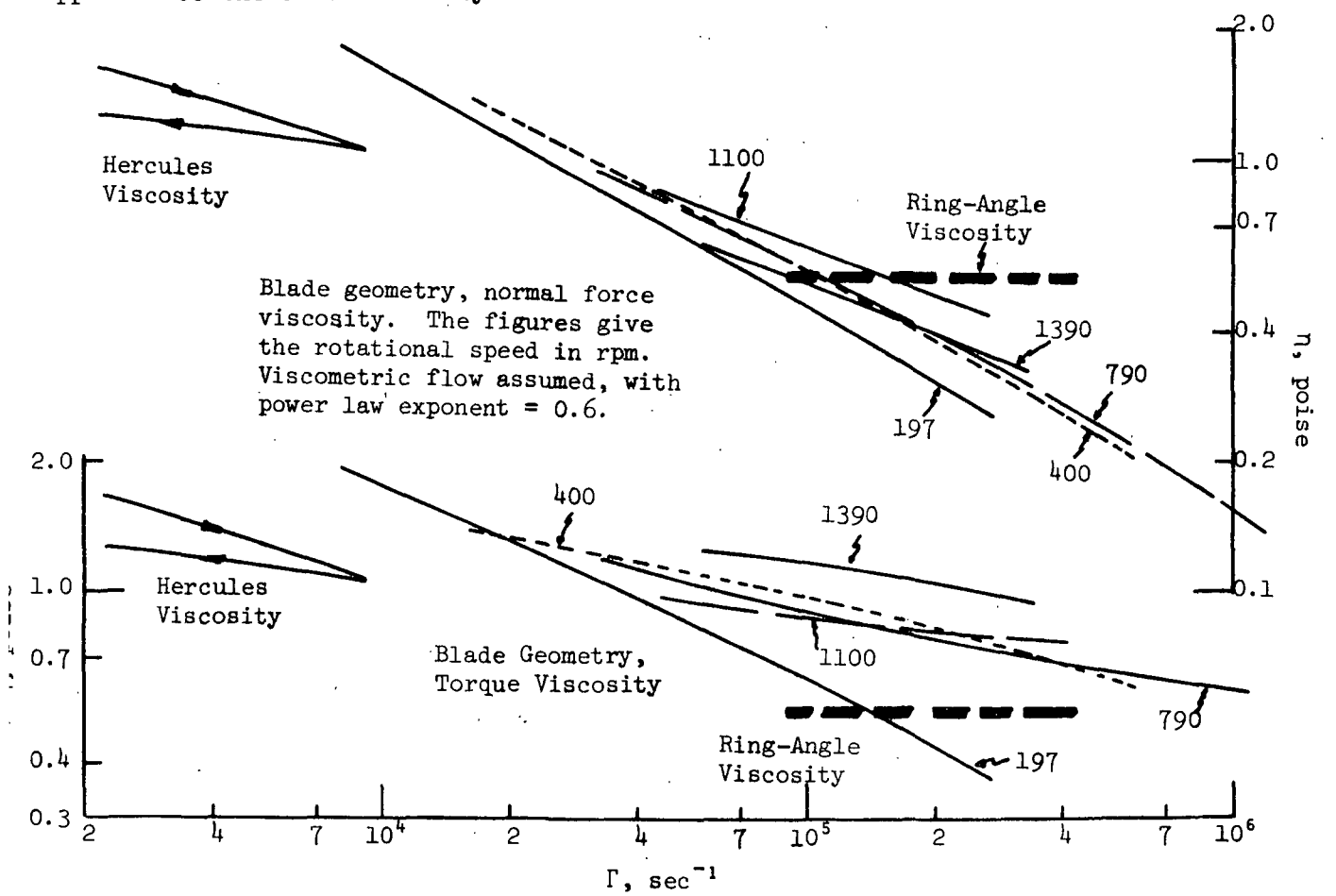

Figure 24. PVA Coating Viscosity Estimated from Blade Geometry Data, Expt. 42

A more direct comparison of results obtained with the circular blade geometry used in the IPC Rheometer and the blade-roll geometry used in the Blade Nip Rheometer can be made by treating basic data and making no assumptions of flow theory or fluid properties. This is done by using the second data analysis technique discussed earlier (p. 36-37).

The technique is based on the following equations:

$$D(V_o,\Delta) = \left(\frac{R_i}{R_o}\right)^2 D(V_i,\Delta) + \frac{2\,T_p}{NR_o^2}\left[1 + 1/2\left(\frac{\partial \log(T_p)}{\partial \log(\omega)}\right)_\Delta\right] \qquad (38)$$

$$F(V_o,\Delta) = \left(\frac{R_i}{R_o}\right) F(V_i,\Delta) + \frac{F_p}{NR_o}\left[1 + \left(\frac{\partial \log(F_p)}{\partial \log(\omega)}\right)_\Delta\right] \qquad (39)$$

Here V_o and V_i are wear plate velocities at the outside and inside of the ring of blades, respectively, T_p and F_p are corrected torque and normal force values obtained with the circular blade geometry, respectively, and N is the number of blades in the circular geometry. It is desired to determine the drag and normal force per blade width at velocity V_o, $D(V_o,\Delta)$ and $F(V_o,\Delta)$, for direct comparison with Blade Nip Rheometer results. The terms containing $D(V_i,\Delta)$ and $F(V_i,\Delta)$ are corrections which account for the blades not extending to the center of the shear plate.

It is first necessary that the data be replotted as $\log(T_p)$ and $\log(F_p)$ vs. $\log(\omega)$ [or $\log(V_o)$], with Δ as the parameter, as is done in Fig. 25. The functions $D(V_o,\Delta)$ and $F(V_o,\Delta)$ are calculated from the curves of Fig. 25 by applying Equations (38) and (39). The trial and error nature of the calculations is due to the necessity of obtaining the corrective terms containing $D(V_i,\Delta)$ and $F(V_i,\Delta)$ from calculated values of $D(V_o,\Delta)$ and $F(V_o,\Delta)$.

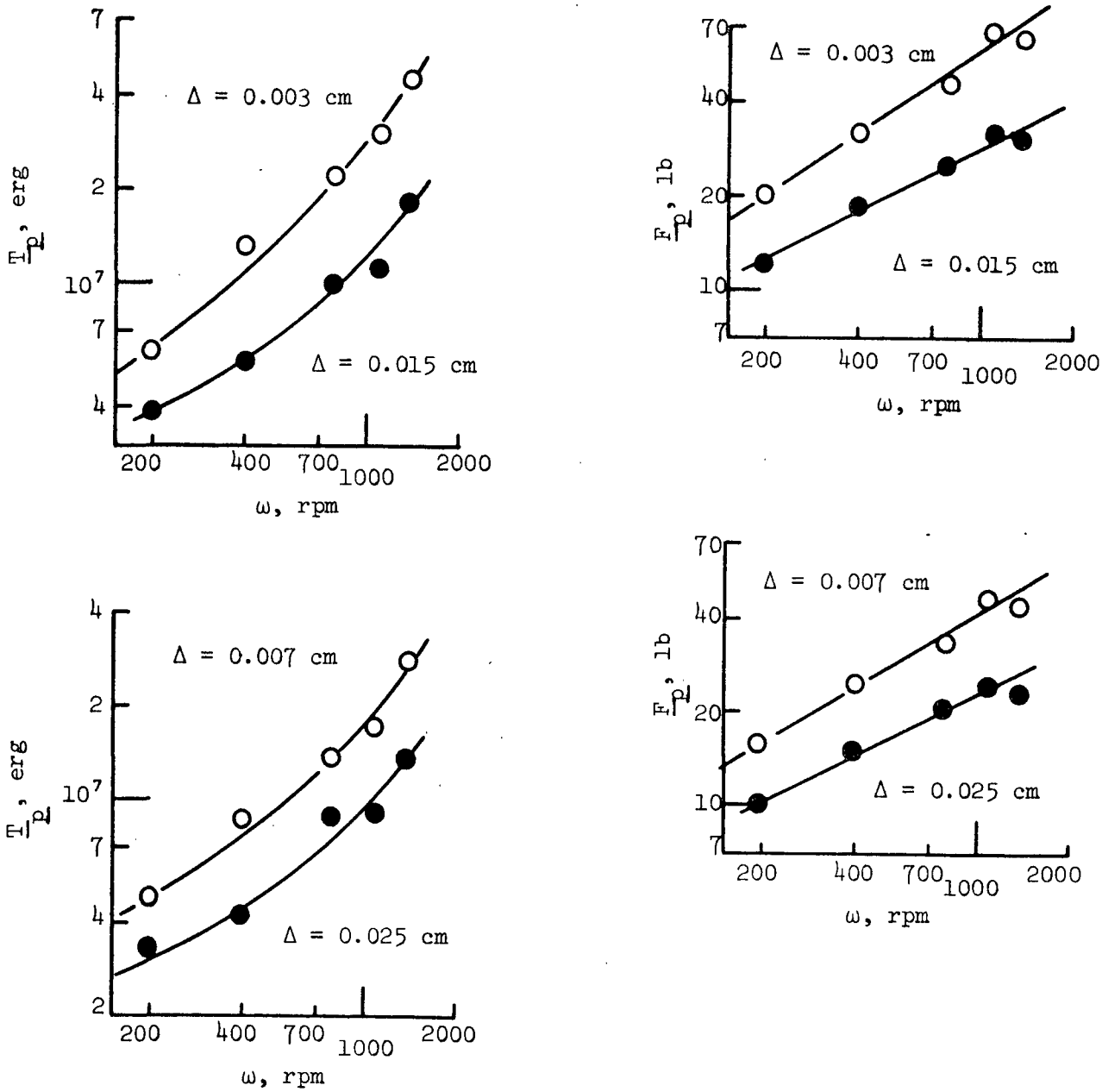

Figure 25. Blade Geometry Data for PVA Coating.
Taken from Fig. 23

Sample calculations are presented in Tables VIII and IX for torque and normal force results, respectively. The following conclusions are drawn from the information presented.

1) The iterative nature of the calculations presents no problems since rapid convergence is obtained.

2) The log-log slope terms in both tables are seen to be of moderate magnitude. It will presumably not be a major source of error for curves sufficiently simple in form.

3) The correction term containing $\underline{D}(\underline{V}_i, \Delta)$ (Table VIII) is very small such that one can extrapolate to low values of $\underline{V}_i$ with minimal error. For the normal force results (Table IX) the corresponding corrections are larger, implying extrapolations may be questionable in some cases.

4) The data presented here are generally simple in form as indicated above. In future analysis of data using these techniques, continual regard must be given to problems which can arise when extrapolated information is required and when the slopes of curves, as well as point values, are used in the analysis.

Drag and normal forces, as determined from the circular blade geometry (IPC Rheometer) and from the Blade Nip Rheometer, are compared in Fig. 26 for comparable PVA coatings. The latter results are for Fluid 21 of Ref. (1). The present results were obtained with blades of tip length 0.225 cm, while the blades on the Blade Nip Rheometer had tip lengths of 0.163 cm. Therefore, only a qualitative comparison of the results can be made. To a small extent for the normal force and a larger extent for the drag, there are seen to be differences in form between the results obtained by the two techniques. Because of the several differences in experimental conditions for the two methods, reasons for

TABLE VIII

DRAG FORCE AS A FUNCTION OF LINER VELOCITY DETERMINED FROM BLADE GEOMETRY TORQUE DATA FOR PVA COATING

ω, rpm	V_o, cm/sec	V_i, cm/sec	T_p, erg	$\frac{2T_p}{NR_o^2}$, erg/cm^2	$\frac{d \log(T_p)}{d \log(\omega)}$	$D(V_o,\Delta)$,[a] dyne/cm	$\left(\frac{R_i}{R_o}\right)^2 D(V_i,\Delta)$, dyne/cm	$D(V_o,\Delta)$,[b] dyne/cm
				Δ = 0.003 cm				
1446	1016	350	4.6×10^7	1.71×10^5	1.43	2.94×10^5	0.07×10^5	3.01×10^5
723	508	173	1.97	0.73	1.06	1.12	0.05	1.17
362	254	87	1.01	0.374	0.85	0.53	0.03	0.56
181	127	44	0.60	0.222	0.75	0.305	0.01	0.32
				Δ = 0.025 cm				
1446	1016	350	1.43×10^7	5.3×10^4	1.36	8.9×10^4	0.3×10^4	9.2×10^4
723	508	173	0.69	2.56	0.84	3.6	0.2	3.8
362	254	87	0.43	1.60	0.60	2.1	0.1	2.2
181	127	44	0.30	1.11	0.44	1.36	0.10	1.46

[a] First estimate.

[b] Second estimate.

TABLE IX

NORMAL FORCE AS A FUNCTION OF LINEAR VELOCITY DETERMINED FROM BLADE GEOMETRY
NORMAL FORCE DATA FOR PVA COATING

ω, rpm	V_o, cm/sec	V_i, cm/sec	F_p, lb	$\frac{F_p}{NR_o}$, lb/cm	$\frac{d \log(F_p)}{d \log(\omega)}$	$F(V_o,\Delta)$, lb/cm	$\left[\frac{R_i}{R_o}\right] F(V_i,\Delta)$, lb/cm	$F(V_o,\Delta)$, [b] lb/cm	$\left[\frac{R_i}{R_o}\right] F(V_i,\Delta)$, [b] lb/cm	$F(V_o,\Delta)$, [c] lb/cm
						$\Delta = 0.003$ cm				
1446	1016	350	73	0.91	0.65	1.49	0.25	1.74	0.29	1.78
723	508	173	46	0.57	0.65	0.93	0.16	1.09	0.19	1.12
362	254	87	29.6	0.37	0.65	0.61	0.11	0.72	0.13	0.74
181	127	44	18.9	0.235	0.65	0.39	0.07	0.46	0.08	0.47
						$\Delta = 0.025$ cm				
1446	1016	350	26.7	0.332	0.49	0.49	0.10	0.59	0.12	0.61
723	508	173	19.1	0.238	0.49	0.35	0.07	0.42	0.08	0.43
362	254	87	13.6	0.169	0.49	0.25	0.05	0.30	0.06	0.31
181	127	44	9.7	0.121	0.49	0.18	0.04	0.22	0.05	0.23

[a] First estimate.

[b] Second estimate.

[c] Third estimate.

the differences in form of the results are not known now. Perhaps future results covering a wider range of gap values, Δ, will be enlightening.

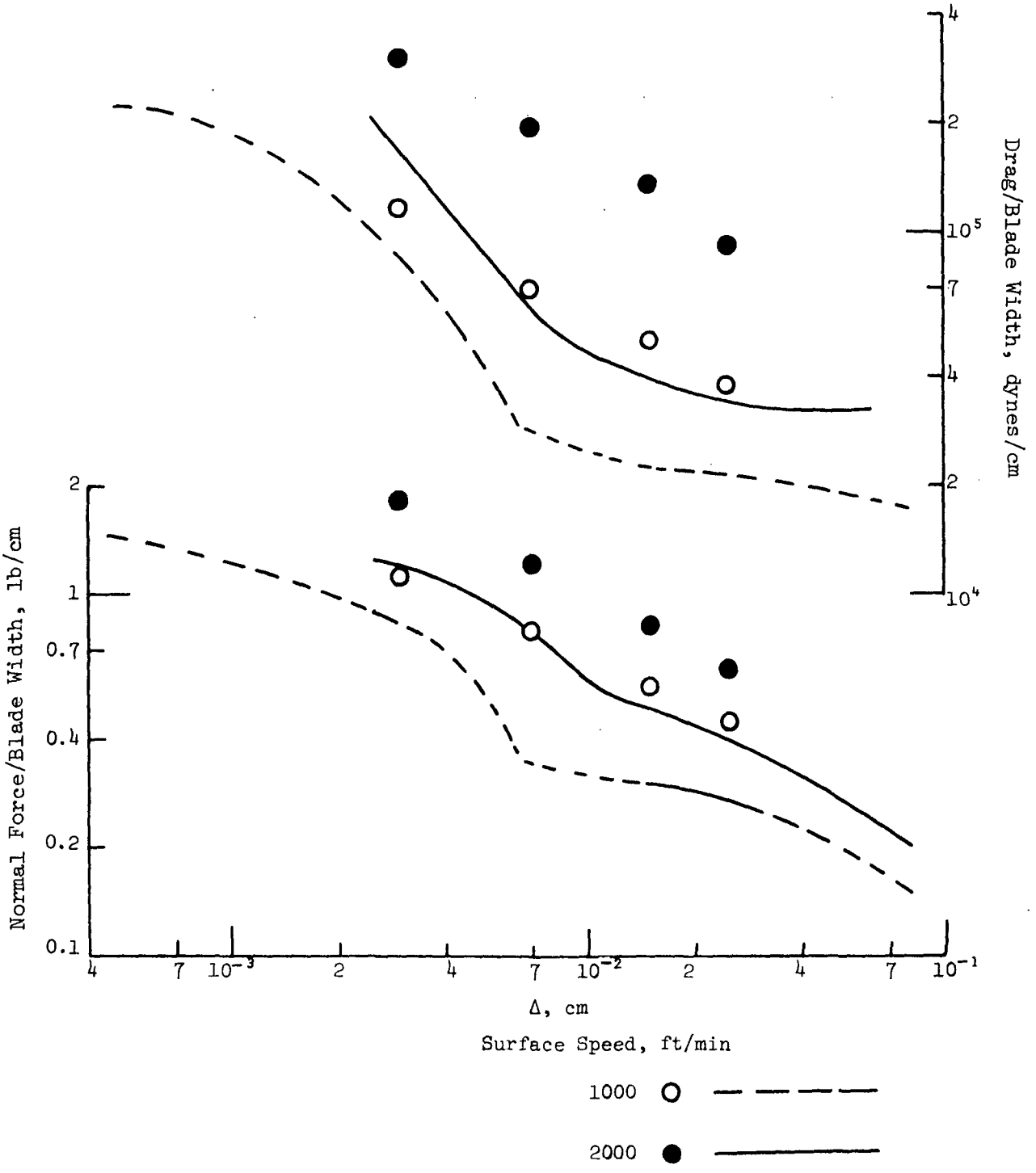

Lines: Data for coating No. 21, Ref. (1), determined with Blade Nip Rheometer.
Circles: Values calculated from data given in Fig. 25, as determined with the IPC Rheometer.

Figure 26. Normal Force and Drag (Tangential Force) per Blade Width for PVA Coating

FUTURE DIRECTIONS

(1) The best means of measuring the viscosity at high shear rates for viscoelastic coatings will be determined. It has been established that the ring-angle geometry is adequate for viscous fluids. For the viscoelastic fluids, the split-ring geometry will be tested first and, if this is not satisfactory, the ring-blade geometry will be tried. The former is preferable since it does not require blade corrections which may require separate measurements.

(2) A program of coating evaluation will be conducted. The goal will be to establish general principles relating formulation to rheological properties.

(3) Duplicate experiments will be made on some standard coatings to determine the magnitude of random error to be expected.

(4) Experiments will be conducted to quantitatively determine the extent of thixotropic breakdown as it occurs in the IPC Rheometer. This is of considerable importance in analyzing rheometer data and, in particular, in translating laboratory results to coater operations.

(5) Work on the revised theory will be continued. While the computer program operates satisfactorily in principle, it has not yet been determined what ranges of variables will produce useful results. Assuming that the viscosity can be determined with one of the viscometric flow geometries, an attempt will be made to determine viscoelastic normal stresses by applying the theory to blade nip results.

DEFINITION OF TERMS

$D(n,\Delta)$ A function relating drag force to viscometric flow in blade nips [see Equation (14)].

$D(v,\Delta)$ Drag force/blade width resulting from blade nip flow [see Equation (27)].

F Normal force applied to shear plate, equals $F_p + F_s$.

F_c Recorder sensitivity setting for normal force measurements.

F_o Zero reading for normal force measurements.

F_p Primary normal force, due to flow between primary shear plate surfaces and wear plate.

F_s Secondary normal force, a corrective term.

$F(n,\Delta)$ A function relating normal force to viscometric flow in blade nips [see Equation (15)].

$F(v,\Delta)$ Normal force/blade width resulting from blade nip flow [see Equation (28)].

H Height of ring sections or blades on shear plate.

n Exponent in power law expression [see Equation (2)].

N Number of blades on blade geometry shear plate.

r Variable radius.

R_i Inside radius of rings or blades on shear plate.

R_o Outside radius of rings or blades on shear plate.

T Total torque resulting from flow in rheometer, equals $T_p + T_s$.

T_c Recorder sensitivity setting for torque measurements.

T_o Zero reading for torque measurements.

T_p Primary torque, due to flow between primary shear plate surfaces and wear plate.

T_s Secondary torque, a corrective term.

v Variable velocity of wear plate surface, a function of rotational speed and variable radius.

LITERATURE CITED

1. Ginn, R. F. A fundamental rheological study of the blade coating process. Project 3069, Progress Report One, The Institute of Paper Chemistry, July 27, 1973.

2. Ginn, R. F. A fundamental rheological study of the blade coating process. Project 3069, Progress Report Two, The Institute of Paper Chemistry, August 9, 1974.

3. Greensmith, H. W., and Rivlin, R. S., Phil. Trans. Roy Soc. A245:399(1953).

4. Ginn, R. F. The measurement of normal stresses in viscoelastic fluids. M.S. Thesis, Univ. Delaware, Newark, Delaware, July, 1963.

THE INSTITUTE OF PAPER CHEMISTRY

Robert F. Ginn
Research Fellow

Gary A. Baum
Group Coordinator

John W. Swanson
Director
Division of Natural
Materials & Systems